ALMA MATER STUDIORUM – UNIVERSITÀ DI BOLOGNA

SCUOLA DI INGEGNERIA E ARCHITETTURA

DIPARTIMENTO DICAM

CORSO DI LAUREA IN CIVIL ENGINEERING LM – INFRASTRUCTURE DESIGN IN RIVER BASINS

TESI DI LAUREA

in

Sustainable Design of Water Resources Systems

Real time flood forecasting for the Reno River (Italy) through the TOPKAPI rainfall-runoff model

CANDIDATO   RELATORE:

NICOLÒ GRINI   Prof. **ALBERTO MONTANARI**

Anno Accademico 2017/2018

Sessione III

Table of contents

1. INTRODUCTION

The occurrence of extreme floods events all around the world makes us pay more attention to their life-threatening, environmental and economic impacts (Guzzetti, Stark, & Salvati, 2005). Consequently, the need emerges to improve the knowledge on flood forecasting techniques as well. To this end, it is necessary to couple the forecasting weather information coming from meteorological models with a rainfall-runoff model which aims to simulate the watershed behaviour within a given catchment.

Traditional physically-based distributed models usually work at a small size and require a large amount of data and lengthy computation times which limit their application in a real-time forecasting scenario. TOPKAPI rainfall-runoff model is an exception as it can be applied at increasing spatial scales without losing model and parameter physical interpretation. Hence, the model represents at the basin scale the soil, surface and drainage network behaviours, following the topography and morphology of the catchment, with parameters values which can be estimated from the small scale. The TOPKAPI model has already been successfully implemented as a research and operational hydrological model in several catchments in the world (Italy, Spain, France, Ukraine, China) (e.g. see Liu and Todini, 2002; Bartholomes and Todini, 2005; Liu et al.,2005; Martina et al., 2006). The study presents the case of the TOPKAPI application on the Reno catchment (northern Italy) in the period between 2005-2013, with the purpose of discuss the reliability of using the model in real-time forecasting configuration and evaluate if it can be considered a possible mean for a more effective torrential watershed management.

The first part of the thesis introduces the problem of flood forecasting in a global prospective and then focuses on the Reno study case. A further introduction of rainfall-runoff models shifts the attention to the general illustration of how the TOPKAPI model works, explaining the main physical principles and assumptions to describe the hydrological and hydraulic processes within the catchment.

The second part of the thesis concerns the Reno case study, describing how its hydraulic, morphologic, topographic, anthropologic and climatic characteristics are implemented in the model and which parameters are calibrated in order to set up correctly the model on the chosen simulation period.

Finally, the last part of the study is dedicated to model implementation on three specific cases. The first test is an analysis of spatial variability aimed at inspecting the effect of rain gauges density; the second consists in empirical approaches trials which define the possibility of predict future rainfall scenario just on the basis of observed measurements. The last test refers to the real-time forecasting application of the model on past events and compare the results obtained with the observed ones in order to evaluate the reliability of the method for flood forecasting. In particular, the second and the third tests are applied to the ten most significant events within the period 2005-2013 (to ensure validity of the results).

2. FLOOD FORECASTING

The global impact of floods is something that cannot be overlooked. Different studies depict the same state of fact: half of the water-related disaster are given by floods. For instance, this is the result of a study conducted by UNESCO among all the types of water-related natural disasters between 1990 and 2001. Sigma World Insurance Database showed the same percentage just regarding 2013 (Sigma, 2013). Even the International Centre for Water Hazards and Risk Management (ICHARM) demonstrated that in the period 1900-2006 the global water-related disasters are the most frequent and threatening among natural hazards. The research, conducted in 2009, pointed out that floods account for the 30% of whole recorded natural disasters and claim the 19% of all the related deaths (ICHARM, 2009). Almost the same tragic percentage (15%) is also reported by UNESCO. An interesting analysis in this study reported that the number of people dead because of flood disasters between 1987 and 1997, in Asia, represents the 93% of all flood related deaths worldwide. If we think that Asian floods are something too far from us to be worried about, we should just take a quick look to the European continent. UNESCO states that also in Europe flash floods have caused many deaths in addition to the more usual ones due to river flooding. The consequences of this type of event get worse especially in mountainous areas.

Flooding is also an economic issue. According to ICHARM the 26% of the natural disasters generating economic losses are floods. For example, the United Kingdom, only in the year 2007, collected an amount of £238 billion losses caused by flood events (United Kingdom Environmental Agency, 2010). Sigma declares that just the 2011 Thailand flood caused $48 billion in losses. For the Bangladesh Water Development Board (Bangladesh Water Development Board, 2009) the cost of flood damages in 2009 was around $750 million in the water sector alone.

Floods, as well as flash floods, can occur anywhere due to a heavy storm or also after a drought period. Indeed, in the latest case, the ground may become so dry

and hard that water cannot penetrate. (World Meteorological Organization). But floods may take place also in other forms. Dikes may flood because of a huge amount of water melted from the snow. In coastal areas floods may be caused by tropical cyclones, tsunamis, tornadoes or thunderstorms. So, everyone is exposed to potentially dangerous flood events and the consequences are worse than we expect.

The increasing awareness of flooding impact has improved in the last decades the practice of flood forecasting and warning.

In particular, **Flood Forecasting** (FF) is the practice by which is possible to predict, with a high degree of accuracy, when and where local flooding will most likely take place. In this way it is possible to warn the authorities and the generic public about the impellent danger as much in advance, and with as much reliability, as possible. This is done using forecasting data, like precipitation and streamflow, processed within models that represent the hydraulic and hydrologic characteristics of the basin. The purpose is to forecast flow rates and water levels for future scenarios, in a range period that goes from a few hours to some days ahead depending on the size of the basin watershed.

Since the 1980s this practice has moved on and evolved from a primacy tendency to control floods with a structural intervention towards a more non-structural approach. In fact, although structural protection measures (e.g. dams and embankments) reduce flood risk modifying flood's characteristics (reducing the peak elevations and the spatial extends), they cannot completely eliminate it. Moreover, these traditional flood management approaches are not feasible for all areas and cause huge environmental impacts. Furthermore, a lot of these infrastructures are old and this means high cost of maintenance and lower level of protection with respect to the one they were designed for. In addition, structural measures are projected according to specific characteristic of the catchment that might change during years: just think about urbanization and climate changes. The result is a higher uncertainty to properly withstand future flood events.

On the contrary, non-structural measures like forecasting provide more reversible and less-expensive mechanisms to reduce flood risk than structural actions (Di Francesco, 2014). This transition is given by the huge technological improvements of instrumentation and remote sensing in the recent years, which are able to monitor the atmosphere and the earth surface. Thanks to this network system it is possible to get real time flood forecasting at regional level: it gives its predictions just few seconds after the meteorological forecasting. The warning procedures start consequently.

Given this importance of flood forecasting in flood warning, it is relevant to specify the difference between the two. Flood forecasting is the ensemble of activities aimed for predicting future discharge and level of the water body. In particular, discharge is generally applied in FF when the maximum discharge that can safely pass through a cross section is known or when dealing with drought forecasting. Water levels instead are required for purposes of evaluating the likelihood of bank failure or to deal with flood detention areas. To the other hand, the concept of **flood warning** defines all those tasks where forecasts are used in order to decide the best way to advice authorities and people about the incoming flood.

2.1 DEFINITIONS IN FORECASTING

One of the most important issues in forecasting is the **Forecasting Lead Time (FLT)**, which can be defined as the minimum required time to successfully implement the actions aimed for reducing risk or appropriately manage the water resources.

Another important issue is the **System Response Time (SRT)**, which can be defined as the time required by the system involved (the catchment, the river reach) to produce significant downstream effects following an upstream input (inflow, rainfall).

Warning time (WT) can be defined as the advance in time with which the warning system is capable of issuing forecasts. It descends from the combination of FLT and SRT and makes it possible to configure the forecasting chain.

In order to understand it, the following examples show two different cases. Firstly, consider a case in which SRT > FLT. This is a common situation faced in large rivers (like Danube or Sava) where the System Response Time is usually high (e.g. 36h) and bigger than the flood forecasting (e.g. 12h) obtained, for instance, just on the basis of a <u>hydraulic model</u>, in which the input is just the measured discharge at the upstream gauge. Therefore WT = SRT, this means that the hydraulic model is just sufficient to give forecast results in time to implement appropriate warning measures.

On the contrary, if we consider a medium\small river (like Reno) the response time of the system decreases drastically (e.g. 8h), ending up with SRT < FLT. In this case forecasting time is no more sufficient to implement flood warning and risk reducing actions. Therefore, there is the need to extend the lead time available. A way to do it is making use of precipitation forecasts within the flood forecasting. This is done by <u>hydrologic models</u>. In fact, these types of models contain all the necessary information to physically represent the catchment. With an additional input of precipitation (which comes initially from observation networks like rain gauges and radar), they can forecast the behavior of water inside the catchment before it reaches the upstream gauge of the river. Adding the new response time of the upstream catchment (e.g. 6h) to the previous river basin, we end up with a total SRT=6h+8h=14h, enough to restore the condition SRT > FLT.

Moreover, in case of flood, warning is required in order to evacuate a large water detention area to be inundated; to do that it is possible to increase even more the SRT with meteorological prediction such as Quantitative Precipitation Forecast (QPF). By the way it is widely recognized that obtaining a reliable QPF is not an easy task, due to the difficulty to forecast rainfall more than other elements of the hydrological cycle. A future interesting perspective is represented by Numerical Weather Predictions (NWP) models. Especially research flood forecasting systems around the world are increasingly moving towards using ensembles of NWPs, called Ensemble Prediction System (EPS). However even if in the literature there are case studies which give encouraging indications that such activity brings added value to medium range flood forecasting, the evidence

6

supporting this is still weak (Cloke, 2009). Moreover, EPS does not seem able to provide accurate rainfall forecasts at the temporal and spatial resolution required by many hydrological applications (Brath, On the role of numerical weather prediction models in real-time flood forecasting, 1999).

2.2 FLOODINGS IN THE RENO CATCHMENT

The study is focused on the Italian scenario of flood forecasting with regard to the Reno catchment in between the northern regions of Tuscany and Emilia-Romagna. Indeed, the mountainous morphology of the Apennines creates the ideal conditions to originate flood events in the lower urbanized plain areas of Emilia-Romagna. In this region the importance of those events was especially recognized in the last decade, in particular from 2010 when the Legislative Decree 49/2010 started a new phase of the national politic approach on the flood risk management, introducing a new and detailed coordination plan with the purpose of reducing the negative health consequences of flood events. Moreover, the frequency that characterized flood events over recent years, has led to an increasing interest and awareness not only for the authorities, but also for mass media and population.

In order to understand the extension and harmfulness of such floods, regional authorities for Po and Reno basin developed maps of flood danger (L. Zamboni, 2015) underling the for each area, within the catchment, the correspondent class of danger: P1 for rare events, P2 for not so frequent events and P3 for frequent events.

By overlapping the map of flood danger (L. Zamboni, 2015) with the Reno catchment boundaries (Fig.1) it is possible to recognize the responsibility of the Reno river in the occurrence of the most frequent flood events in the plain regions. Considering the typical characteristics of torrential rivers such as the Reno one (narrow river bad and steep slopes given by the mountain morphology of Apennines, high difference in elevation (almost 1900m) between the origin and the outlet just 60 km distant from each other), the result is that in case of heavy rain event over mountainous areas, the water flows forcefully and rapidly toward the plan fields in a quantity that may be so large to become a real danger

for activities and people living in those areas. The response time of the torrent system is so short that it may happen that hazardous discharges arrive on lowlands even before the precipitation that originates them in the mountains. In this scenario, it becomes extremely relevant to find methods that allow an extension of the lead-time of the river flow forecast, such as QPFs, which may enable a more timely implementation of warning systems to face the torrential events is safe conditions.
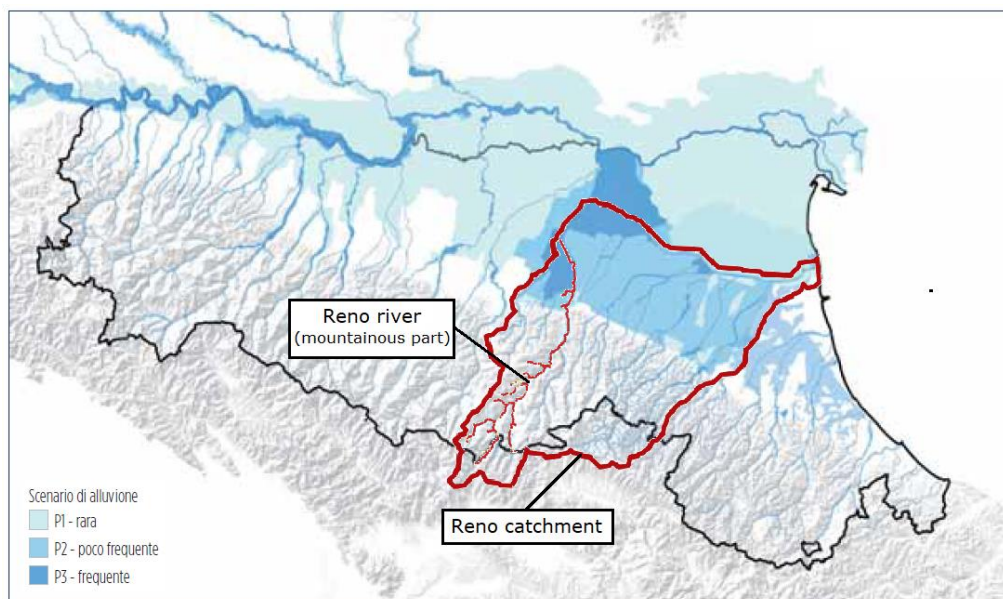

Fig.1 - Map of flood danger in Emili-Romagna. The Reno catchment and the Reno river are highlighted

3. RAINFALL-RUNOFF MODELS

Rainfall-Runoff (RR) model is a mathematical model which can simulate the relationship between the rainfall event over a catchment and the consequent river discharge. In simply words the model calculates the conversion of rainfall into runoff. The purpose is to get the river flow hydrograph given by an observed (or forecasted) rainfall event.

3.1 HISTORY OF RAIFALL-RUNOFF MODELS

Just to give a brief historic overview about the RR models development: the 1932 is widely recognized as the date in which the first rainfall runoff model was born. It was the so-called Unit Hydrograph: a technique providing a practical and relatively easy-to-apply tool to quantify the watershed response (in terms of runoff volume and timing) to a unit input (e.g. one cm) of rainfall. This is done through two strong hypotheses: rainfall event is uniformly distributed over the watershed and runoff response is linear and time-independent. Someone may argue that Rational Method was formulated firstly, in 1850, but considering the fact that it is not able to estimate the flow volume but just its peak value, we think that it based on too simple assumptions to be considered as a RR model.

The Linear Reservoir Model represents a step forward. Indeed, it considers the energy balance conservation to establish the relationship between the storage and the runoff of a catchment. By the way, in order to solve the system of equations, the hypothesis of linearity is necessary: a too strong assumption for the purpose of representing the physical behaviour of the catchment.

Therefore, all these models are based on strong hypotheses and are reliable just for small and impervious catchments. In order to achieve a better physical interpretation of catchment response, the 1960s saw the development of Conceptual Models in which the basin is treated as an only entity with parameters that characterize its global behaviour. Moreover, the hydrologic cycle is represented by individual components that simulate the response of a particular subsystem. However, considering that those parameters were physically meaningless, there was the need to go ahead.

At the end of 1970s a new type of lumped model was introduced, based on the idea that rainfall-runoff process is mainly dominated by the dynamics of saturated areas. This is represented by a two-parameter distribution function curve representing the relation between the total volume of water stored in the soil and the extension of the saturated area (e.g. HYMOD model). Other processes represented in the model (drainage, percolation, groundwater flow, etc.) are based on empirical parameters that have to be estimated from data.

The need to directly relate parameters with measurable quantities brought Beven and Kirkby in 1979 to elaborate a more physically meaningful distribution function model, the so called TOPMODEL. But the physically based hypothesis proved to be true only for very small hill-slope catchments (Franchini M., 1996).

Therefore, Freeze and Harlan proposed a mathematical model based on distributed physical knowledge of surface and subsurface phenomena. In fact, by a numerical integration of the coupled sub-systems (surface flow, unsaturated and saturated subsurface flow) and by matching the solutions of each sub-system with the boundary conditions of another, a catchment scale prediction could be produced. But the cost to pay was the calibration of too many parameters.

More recently, the wider availability of distributed information (radar rainfall, soil types, land cover, etc.) has facilitated the production of simplified physically meaningful distributed hydrological models (like TOPKAPI). These models, based on simplified assumptions (coupling conceptual and physical approaches) can be applied successfully to flood forecasting. In conclusion since the majority of models were developed after '90s, we can consider RR model application as a young science and therefore as a very active field of research.

3.2 HOW RAINFALL-RUNOFF MODELS WORK

The following sub-chapter is aimed to explain the basic concepts behind the functioning of rainfall-runoff model. By understanding these principles, we will realize how complex hydrological RR models as TOPKAPI work.

The mathematical model is nothing else than a system of equations in a number which is proportional to the number of variables that we want to simulate

(**constitutive equations**). Therefore, we need a minimum number of equations which is equal to the number of unknowns. Usually in this type of model variables are functions of time, since we want to simulate the behaviour of the catchment evolving in time. Hence, the final river flow output is not only a function of rainfall but also a function of time, therefore we consider it as a **dynamic model**. Otherwise in order to simulate the variables we are interested in, we may need to consider the **state of the system**. The latter one considers the hydrologic condition of the catchment at the time of the rain event (like drought and saturated conditions) and the variable which describe this is the storage. This relationship among variables: rainfall $P(t)$ (input), river flow $Q(t)$ (output) and storage $W(t)$ (state of the system), can be conceptually associate with a bucket model (Fig. 2)
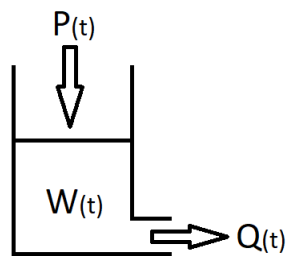

Fig.2 – conceptual association between the catchment and the bucket model

The amount of storage quantifies the state of the catchment: if $W(t)=0$ the catchment is dry, on the contrary if it reaches its maximum potential value the basin is completely saturated. Therefore, storage is a state variable and the introduction of it is necessary if we want to take into account the state of the catchment, thus two equations are needed for this specific case. Of course, the concept can be extended and the complexity of the model increases taking into account other states of the catchment, introducing additional state variables and equations.

Given that the purpose of this model is to describe the movement of water within the water cycle, equations are explicitly or implicitly based on physic laws. Examples of these equations are the conservation of energy, conservation of

mass and conservation of momentum. Moreover, by adding laws of chemistry, ecology, social science and so forth, it is possible to increase the complexity of the model taking into account other factors to better describe the dynamics of the catchment (changes in land-use/landcover, inclusion/removal of infrastructure, etc.)

Beside variables, constitutive equations may include **parameters**. They are numeric factors within the equations used in the model, which can assume different values in order to give flexibility to the model itself. To find the best value, for each parameter, that better describes the catchment it is necessary to calibrate the model. Nevertheless, in some models, parameters do not have a single fixed value, but they may change during the simulation depending on time or state of the system.

3.3 RAINFALL-RUNOFF MODELS CLASSIFICATION

The RR models used for flood forecasting may be classified in different categories. They can be distinguished basing on the way catchment processes are represented:

- **Deterministic model**: compute several equations representing the different watershed processes that produce a single model output for a given set of parameters;
- **Stochastic model**: provide the capability to simulate the random and probabilistic nature of inputs and responses that govern river flows.

Deterministic model may be subdivided also according to the representation of the hydrological process within the catchment:

- **Physically based model**: the process of transformation of rainfall into runoff is time dependent and is function of the physical characteristics of the catchment.
- **Conceptual model**: describe the rainfall-runoff process in a more abstract and general way with respect to the physically based approach. In this way it has a simpler structure and more linearity in variables and parameters changes.

- **Synthetic** (or **empirical** or **black-box**) **model**: its purpose is not aimed to mathematically represent hydrologic and physical phenomena in the catchment. It considers the system as a closed box (black-box) on which there are specific hypothesis. Therefore, the model searches the mathematical operator that links rainfall to runoff in the best way possible.

An additional subdivision regards the spatial distribution of inputs and parameters:

- **Lumped model**: conceptualizes the catchment as a set of various storage tanks which represent different water storages within the catchment (superficial, unsaturated and groundwater zones). The model describes how the water moves through these tanks with a set of expressions;

- **Distributed model**: the catchment is divided in cells. For each one of them the basin properties are represented with specific parameters for that particular cell. In this way distributed model generally reproduces the hydrological processes within the catchment in a spatially-varied way.

Further classification account for the estimation of the rainfall for the lead time:

- **Updating model**: involves the use of real-time data as input of the model. In this way the model is more accurate and more reliable.

- **Non-updating model**: uses the rainfall input just on the basis of observed data.

It is important to state that the above classifications are not rigid and it is difficult to assign unequivocally a model just to a category.

4. TOPKAPI MODEL

TOPKAPI is an acronym which stands for **TOP**ographic **K**inematic **AP**proximation and **I**ntegration. It is a fully distributed model in the sense that it considers the catchment with a grid cell discretisation for each of which the structure of the model is applied. The term physically based is used because of the capability of the model to represent on the catchment the hydrological processes described by the fluid mechanics and soil physics. The input parameters required are relatively few (15), only three or four of which typically require calibration (Liu & Todini, 2002). The chapter presents the main aspects of the model concerning its principles and physical concepts.

4.1 STRUCTURE AND METHODOLOGY

The model is based on the idea of combining the kinematic approach with the topography of the catchment. The Digital Elevation Model (DEM) subdivides the basin domain in squared cells, whose size generally increases with the overall dimension of the basin (pixel size is generally between 100 and 1000m). Therefore, the drainage network is evaluated according to the principle of minimal energy cost (Band, 1986) comparing the elevation of each cell with the ones of its neighbourhood cells. In particular, according to the TOPKAPI **eight direction scheme**, the links between the active cell and the eight surrounding is evaluated: the active cell is assumed to be connected downstream with a sole cell, while it can receive upstream contributions up to seven cells. In this way flow paths and slopes are evaluated. Moreover, for every grid cell of the DEM is assigned a value for each of the physical characteristics (parameters) represented in the model. Therefore, the spatial distribution of parameters, the precipitation input and the hydrological response are described in the horizontal direction by the grid scheme just obtained and in vertical by a column of soil for each grid square.

TOPKAPI proposes a single layer soil model in which the soil is considered with a limit thickness (usually 1 or 2 meters) and high hydraulic conductivity (because of the macro pores structure of the top layer soil). It contributes to the horizontal

flow (surface runoff) if its soil moisture content exceeds its saturation level (Todini E. , 1995), otherwise if its moisture content exceeds its field capacity, it loses water by percolation toward the deeper soil. The model does not consider the mechanism of infiltration at that depth and the consequently recharge to aquifers, the reason is that typically deep groundwater flows are long time events and their contribution to surface discharge of the catchment is observable only in a long-time scale (years). Therefore, since this study considers the discharge behaviour of the catchment on a shorter temporal window, it is reasonable to consider the water which exits from the soil cell (percolation) as lost from the model. The following conceptual scheme depicts the main structure of the model (Fig.3) regarding the interactions among three main reservoirs. The components of evapotranspiration, snowmelt and percolation will be discussed further.

TOPKAPI is constructed around seven components: surface flow, groundwater flow, channel flow, evapotranspiration, snowmelt, percolation as well as lake/reservoir routing (this one is not considered in the present study). All the components may be considered for each grid cell of the DEM. The model is based on the hypothesis that sub-surface flow, overland flow and channel flow can be approximated using a **Kinematic Wave Approach**. The integration in space of the consequently non-linear Kinematic Wave equations, representing the three horizontal flow components (sub-surface, overland and channel), results in three "structurally-similar" non-linear reservoir differential equations (Liu Z. , 2002).

4.2 MODEL ASSUMPTIONS

The TOPKAPI model is based on 6 fundamental assumptions:

1. Precipitation is constant over the single grid cell, by means of area-distribution techniques (Thiessen polygons and Black Kriging)
2. All the precipitation falling on the soil infiltrates into it, unless the soil in a particular zone (intended as cell) is already saturated: the saturation runoff mechanism, often called Dunne Mechanism (T.Dunne, 1978).

3. The slope of the water table coincides with the slope of the ground. This is the fundamental assumption of the Kinematic wave approximation in the Saint-Venant equation. Indeed, the model adopts the Kinematic wave propagation equation to describe the behaviour of horizontal flow in the unsaturated areas.

4. Local transmissivity, like horizontal subsurface flow in a cell, depends on the integral of the total water content of the soil in the vertical direction.

5. In the soil surface layer, the saturated hydraulic conductivity is constant with depth and, because of macro-porosity, is much larger than that of deeper layers.

6. During the transition phase, the variation of water content in time is constant in space.

4.3 MODEL EQUATIONS

The equations that for each cell define the interactions among the three main reservoir (soil, overland and channel reservoirs) are obtained by combining the physically-based and mass continuity equations under the approximation of the kinematic wave approach. The achieved differential equations are then analytically integrated in space to the finite dimension of the grid cell. For a fully detailed description of the theory which stands behind the resolution of these equations, it is suggested the analysis of the papers written by Liu and Todini (Liu & Todini, 2002). Just an overview aimed to understand the main relationship between equations is discussed below.

For each of the three reservoirs, the equation of mass continuity (of which a generic cell i is composed) can be written as a classical differential equation of continuity:

$$\frac{dV_i}{dt} = Q_i^{IN} - Q_i^{OUT} \tag{1}$$

where:

- V_i : total volume stored in the reservoir
- $\frac{dV_i}{dt}$: water storage development in time

- Q_i^{IN} : total inflow contribution to the reservoir
- Q_i^{OUT}: total outflow contribution to the reservoir

The assumption of kinematic wave approximation leads to neglect the acceleration terms in the Saint-Venant energy equation and therefore it is possible to resolve the continuity and mass balance equations by assuming a non-linear relationship between Q_i^{OUT} and V_i transforming Eq. (1) into an Ordinary Differential Equation (ODE):

$$\frac{dV_i}{dt} = Q_i^{IN} - b_i V_i^\alpha \tag{2}$$

where:

- Q_i^{IN} : combination of the forcing variables which are depending on the reservoir type (soil, overland, channel). Represents the interconnecting flows between the element storage reservoir (cell) with upstream connected cells, including rainfall and evapotranspiration.
- b_i : function of geometrical and physical characteristics of the reservoir
- α : function of geometrical and physical characteristics of the reservoir

For each cell, at each time-step t of the simulation, the Q_i^{IN} inflow rate is computed, assuming that it is constant over the whole interval Δt, then the Eq. (2) is solved by numerical integration. The method used by TOPKAPI to solve the ODE equation is a hybrid approach between the Runge-Kutta-Fehlberg (RKF) method and the quasi-analytical solution (QAS). The RKF is used because of its adaptive time step algorithm that is widely recognised as one of the most numerically stable algorithms to solve ODEs equations in forward difference mode (Weatley, 1994). Moreover, its additional function, with respect to the original Runge-Kutta algorithm, allows to estimate the error at each computational step. To the other hand the QAS method is proposed by Liu and Todini (2002) because of its quicker computational time with respect to RKF. Therefore, the hybrid method is based on the QAS method as default procedure, and switches to the RKF algorithm when the mass continuity equations (Eq.(1)) are not satisfied. In this way it is possible to reduce the computation time of more than 50% compared with a RKF application used on its own. Table 1 shows for

each reservoir all the variables that are computed from the ODE. In order to
better understand the connections among reservoir inflows and outflows, the
Fig.3 illustrates the scheme of a typical modelled cell (note that for sake of clarity
the figure neglects the evapotranspiration processes).

Drainage coefficient

In situations where a grid cell is described by a slope ($tan\beta_1$) in direction
x and a different slope ($tan\beta_2$) in direction y (Fig.3), the local
conductivity coefficient C (which defines the value of b factor in the
Eq.(2)) is multiplied by a drainage coefficient σ:

$$\sigma_S = 1 + \frac{tan\beta_2}{tan\beta_1} \qquad \text{Soil Drainage Coefficient}$$

$$\sigma_O = 1 + \left(\frac{tan\beta_2}{tan\beta_1}\right)^{\frac{1}{2}} \qquad \text{Overland Drainage Coefficient}$$

The coefficient is automatically computed by TOPKAPI on the basis of
pixel elevation. The use of drainage coefficients increases the amount of
water moving either in the sub-surface soil layer and on the surface; as a
consequence, the amount of water that gets into the drainage network
increases too.

Flow partition coefficient (F$_P$)

The total outflow from the soil and from the overland ($Q_S^{OUT} + Q_O^{OUT}$) is
partitioned between the downstream cell and the channel network
according to the flow partition coefficient (F_P). It represents the
percentage of soil and overland flow flowing toward the channel, namely
in the direction that is perpendicular to that of the channel and parallel to
that of the outflow pixel. In the study it has been decided to assign the
value of 0.5 to the flow partition coefficient in order to split in half the
outflow of either soil and overland reservoirs.

Tab.1 - Variables computed at each cell i between time t and Δt:

|	$V(t)$	Input value — Coefficient b	Input value — $Q^{IN}(t, t+\Delta t)$	ODE solution $V(t+\Delta t)$	Outflow discharge $Q^{OUT}(t, t+\Delta t)$	Flow partitioning — Flow rate to the next cell during $(t, t+\Delta t)$
Soil	$V_{S_i}(t)$	$b_i = \dfrac{C_{S_i} X}{X^2 \alpha_S} \qquad C_{S_i} = \dfrac{L_i K_{S_i} \tan(\beta_i)}{(\theta_{s_i} - \theta_{r_i})^{\alpha_S} L_i \alpha_S}$ X : lateral dimension of cell grid [m] L_i : soil depth [m] K_{S_i} : saturated hydraulic conductivity [m/s] β_i : ground slope angle [degrees] θ_s : saturated soil moisture content [cm³/cm³] θ_r : residual soil moisture content [cm³/cm³] α_S : power coefficient = 2/5 [dimensionless]	$Q_{S_i}^{IN} = P_i X^2 + \displaystyle\sum_{j=1}^{n^\circ up_{cells}} (1 - F_P)\left(Q_{S_j}^{OUT} + Q_{O_j}^{OUT}\right)$ P : precipitation intensity [m/s] X : lateral dimension of cell grid [m] $n^\circ\, up\_cells$: total number of contributing upper cells X_c : channel length [m] Fc : flow partition coefficient	$V_{S_i}(t+\Delta t)$	$Q_{S_i}^{OUT} = Q_{S_i}^{IN} - \dfrac{V_{S_i}(t+\Delta t) - V_{S_i}(t)}{\Delta t}$	To the next soil reservoir: $Q_{S_i}^{OUT} - Q_{S_i}^{excess} - F_P \cdot Q_{S_i}^{OUT}$
Overland	$V_{O_i}(t)$	$b_i = \dfrac{C_{O_i} X}{X^2 \alpha_o} \qquad C_{O_i} = \dfrac{1}{n_{o_i}} \sqrt{\tan(\beta_i)}$ X : lateral dimension of cell grid [m] n_{o_i} : Manning's roughness coefficient [m$^{-1/3}$s^{-1}] β_i : ground slope angle [degrees] α_o : power coefficient = 5/3 [dimensionless]	$Q_{O_i}^{IN} = Q_{S_i}^{excess} = \max(0, Q_{S_i}^{OUT} - Q_{S\,maxi})$ $Q_{S\,maxi} = X K_{S_i} L_i \tan(\beta)$ X : lateral dimension of cell grid [m] L_i : soil depth [m] K_{S_i} : saturated hydraulic conductivity [m/s]	$V_{O_i}(t+\Delta t)$	$Q_{O_i}^{OUT} = Q_{O_i}^{IN} - \dfrac{V_{O_i}(t+\Delta t) - V_{O_i}(t)}{\Delta t}$	To the next soil reservoir: $Q_{O_i}^{OUT} - F_P \cdot Q_{O_i}^{OUT}$
Channel	$V_{C_i}(t)$	TRIANGULAR CROSS-SECTION $b_i = \dfrac{(sen\gamma)^{2/3}}{2^{2/3}(\tan\gamma)^{1/3} \alpha_c} X \qquad C_{C_i} = \dfrac{1}{n_{c_i}} \sqrt{\tan(\beta_{C_i})}$ X : lateral dimension of cell grid [m] γ : angle riverbad n_{c_i} : Manning's roughness coefficient for channel flow [m$^{-1/3}$s^{-1}] β_{C_i} : channel slope angle [degrees] α_c : power coefficient = 4/3 [dimensionless]	$Q_{C_i}^{IN} = Q_{C_i}^{UP} + F_P\left(Q_{S_i}^{OUT} + Q_{O_i}^{OUT}\right)$ Q_C^{UP} : outflow rate of the previous upper river cell Fc : flow partition coefficient	$V_{C_i}(t+\Delta t)$	$Q_{C_i}^{OUT} = Q_{C_i}^{IN} - \dfrac{V_{C_i}(t+\Delta t) - V_{C_i}(t)}{\Delta t}$	To the next channel reservoir: $Q_{C_i}^{OUT}$
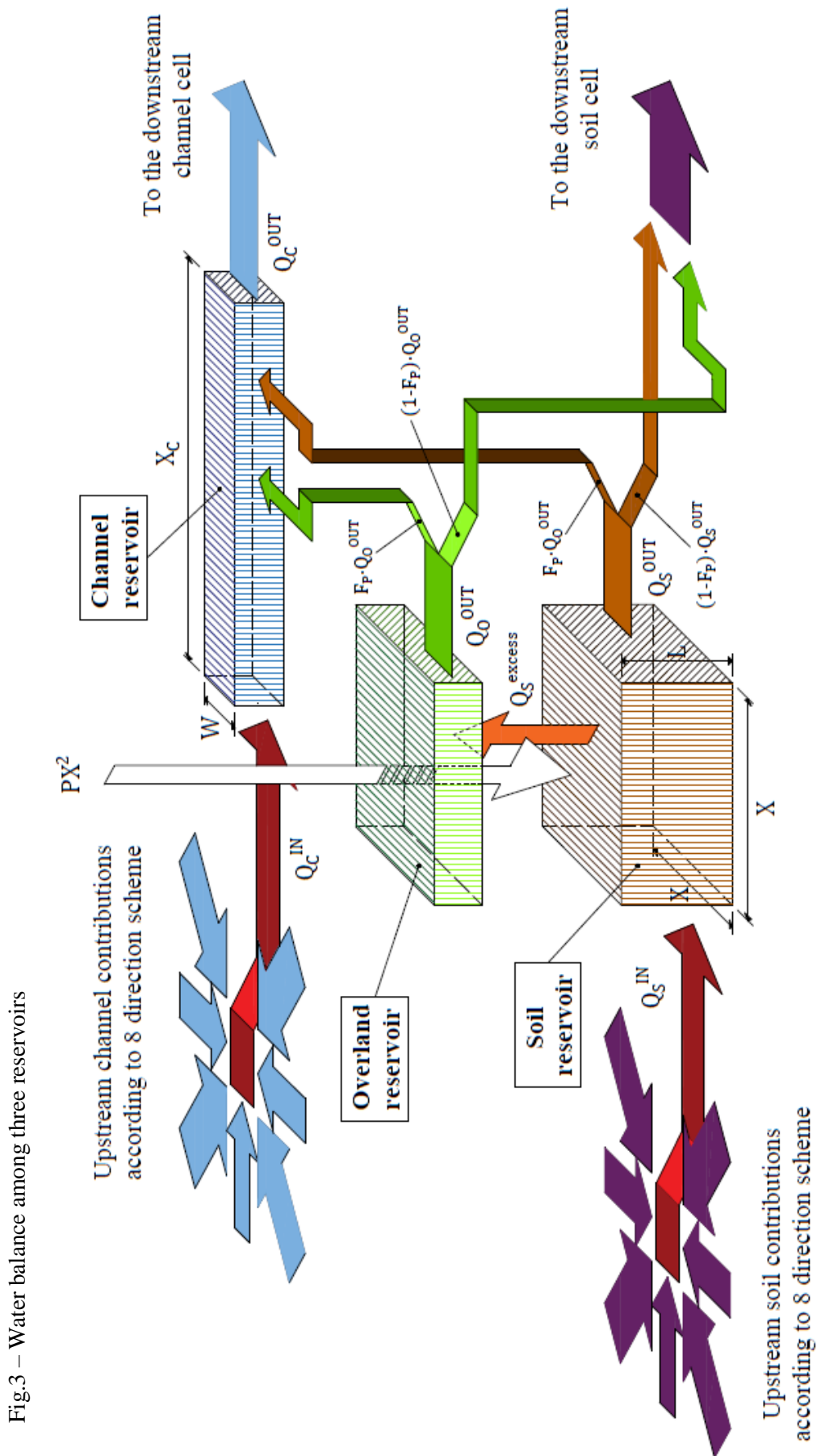
Fig.3 – Water balance among three reservoirs

4.4 EVAPOTRANSPIRATION COMPONENT

The most physically realistic model for estimating actual evapotranspiration is the Penman-Monteith equation, which has been widely used in many distributed models. However, due to the difficulty to get real-time data for Penman-Monteith estimations in operative flood forecasting applications, a simplified approach is generally necessary. Indeed, evapotranspiration plays a major role not in terms of its instantaneous impact, but in terms of its cumulative temporal effect on the soil moisture volume depletion; this reduces the need for an extremely accurate expression, provided that its integral effect is well preserved.

Therefore, a simplified empirical equation such as the Thornthwaite method is used to get the reference potential evapotranspiration **ET₀**, computed on a monthly basis:

$$ET_0(m) = 16 \, a(m) \left[10 \frac{T(m)}{b(m)} \right]^c \tag{3}$$

with:

$$a_M = \frac{n_M}{30} \frac{N_M}{12}$$

$$b_M = \sum_{M=1}^{12} \left[\frac{T_M}{5} \right]^{1.514}$$

$$c = 0.49239 + 1792 \cdot 10^{-5} b - 771 \cdot 10^{-7} b^2 + 675 \cdot 10^{-9} b^3$$

where:

- $ET_0(m)$: reference potential evapotranspiration in the month m
- $T(m)$: average air temperature in the month m
- $N(m)$: maximum number of sunshine hours in the month m
- $n(m)$: number of days in the month m
- $m = 1,2, \dots, 12$ [months]

The developed relationship is linear in temperature and permits the desegregations of the monthly results on a daily or even on an hourly basis.

Once ET_0 has been computed on a monthly basis, the following empirical equation is used to relate it to the compensation factor W_{ta}, the average temperature (recorded) of the month T and the maximum number of hours of sunshine N of the month.

$$ET_0(m) = \beta(m) \, N(m) \, W_{ta}T(m) \tag{4}$$

where:

- $T(m)$: monthly-average ait temperature in the month m
- W_{ta} : weighting factor for the radiation effects
- $N(m)$: maximum number of sunshine hours in the month m
- $m = 1,2, \dots, 12$ [months]
- $\beta(m)$: regression coefficient for the month m

Once the values of coefficient β is obtained for each month m, the values of T, W_{ta}, N and β itself can be now used to estimate ET_0, instead of Thorntwaite formula. In particular β is used to obtain the potential evapotranspiration values (**ET$_P$**) by a simplified equation derived from the radiation method (Doorenbos J. P., 1984).

$$ET_P = ET_0 \cdot K_{C_{crop}} \tag{5}$$

In particular since we are interested to obtain the ET_P value for each cell, for each month of the year, for any crop at any time step Δt, Eq.(5) becomes

$$ET_P = [\beta \, N \, W_{ta}T_{\Delta t}] \cdot K_{C_{crop}} \cdot \frac{\Delta t}{30 \cdot 24 \cdot 3600} \tag{6}$$

where:

- Δt : time interval [s]
- $K_{C_{crop}}$: crop factor
- $T_{\Delta t}$: average air temperature over the cell i in Δt [°C]

For different types of land use, monthly crop coefficients are given, reflecting the state of the plants in annual growth cycle (Doorenbos & Pruitt, 1992).

In fact, different evapotranspiration capacities of land uses are affected by the transpiration and evaporation from the water intercepted by the given vegetation.

Finally, the potential evapotranspiration value is corrected as a function of the actual soil moisture content to obtain the actual evapotranspiration (**EP$_A$**).

$$ET_A = \begin{cases} ET_P \dfrac{V}{\beta V_{sat}} & for\ V \leq \beta V_{sat} \\ ET_P & elsewhere \end{cases} \tag{7}$$

where:

- V : actual volume of water stored into the soil [m^3]
- V_{sat}: local saturation volume [m^3]
- β : percentage of the saturation volume

The evapotranspiration losses are taken in account by the model by subtracting them both from the channel outflow rate, and from the soil or overland outflow depending on saturation conditions: if the cell is fully saturated evapotranspiration is taken off from the overland outflow rate, on the other hand evapotranspiration is extracted from the soil store alone. In particular:

$$ET_A = \begin{cases} ET_P \dfrac{V}{\beta V_{sat}} & for\ \ soil/overland\ ratio \\ ET_P & for\ channel\ ratio \end{cases}$$

4.5 SNOWMELT COMPONENT

For reasons of limited data availability, the snowmelt module within TOPKAPI is driven by a radiation estimate based upon the air temperature measurements; in practice, inputs to the snow module are precipitation, air temperature, and the same radiation approximation which was used in the evapotranspiration module. The principle is that as precipitation falls on the catchment, the snow accumulation and melting component identify the amount of water that actually reaches the soil surface.

At each model pixel snowmelt is computed by following five steps, on the basis of a snow pack energy and mass balance.

1. Net solar radiation estimation

The estimation of the radiation for each DEM grid (Eq.(8))is performed by re-converting the latent heat (which has already been computed previously as the reference evapotranspiration ET_0) to radiation (Eq.(9)).

$$Rad = \lambda ET + H \tag{8}$$

where:

- Rad : net solar radiation
- λET : latent heat flux
- H : sensible heat

$$\lambda ET = C_{er} \cdot ET_0 \tag{9}$$

with:

$$C_{er} = [606.5 - 0.695(T - T_0)]$$

where:

- C_{er} : conversion factor [Kcal/Kg]
- T_0 : fusion temperature of ice [273 °K]
- T : air temperature [°K]
- ET_0: potential reference evapotranspiration

According to empirical tests applied within the TOPKAPI approximations, it is possible to compute the sensible heat as:

$$H = \lambda ET \tag{10}$$

Therefore:

$$Rad = 2 \cdot [606.5 - 0.695(T - T_0)]ET_0 \tag{11}$$

In addition it is necessary to account for another factor which plays an extremely important role in snowmelt: Albedo. It is taken into account by which an efficiency factor η (a function of Albedo).

$$Rad = 2 \cdot \eta \cdot [606.5 - 0.695(T - T_0)]ET_0 \tag{12}$$

24

Albedo (or reflection coefficient) is the diffuse reflectivity, or reflecting power, of a surface. It is the ratio of reflected radiation from the surface to incident radiation upon it. It is dimensionless and it is measured on a scale from zero (for no reflection of a perfectly black surface) to 1 (for perfect reflection of a white surface). In TOPKAPI model an average Albedo value is used to compute the efficiency factor η for clear sky and overcast conditions according to the following empirical equations:

$$\eta_{clear} = 1 - Albedo$$

$$\eta_{overcast} = (1 - Albedo) \cdot 1.33$$

Default value is Albedo=0.4, which brings η=0.6 for clear sky (when not raining or snowing) and η=0.8 for overcast conditions (when raining or snowing).

2. Estimation of solid and liquid precipitation amount

On the basis of air temperature, TOPKAPI estimates the percentage of liquid precipitation using the following function:

$$Rain_{\%}(T) = \frac{1}{1+e^{\frac{T_{AIR}-T_S}{0.6}}} \tag{13}$$

where:

- T_S : threshold temperature, fixed to 0°C
- T_{AIR} : air temperature

3. Estimation of the water mass and energy budgets based on the hypothesis of zero snowmelt

A tentative value for mass and energy of the snowpack is computed at time $t + \Delta t$ (with the hypotesis of zero snowmelt):

Tentative mass balance : $Z_{t+\Delta t}^* = Z_t + P$ $\tag{14}$

Tentative energy balance:

Snow: $E_{t+\Delta t}^* = E_t + Rad + C_{si}TP$ $\tag{15}$

$$\text{Rain: } E^*_{t+\Delta t} = E_t + Rad + \left[C_{si}T_0 + C_{lf} + C_{sa}(T - T_0)\right]P \quad (16)$$

where:

- Z_t : water equivalent mass at time t [mm]
- P : precipitation [mm]
- E_t : energy at time t [mm]
- Rad : net solar radiation
- C_{si} : specific heat of ice $\left[= 0.5 \, {}^{Kcal}/_{{}^\circ K \cdot Kg}\right]$
- C_{lf} : latent heat of fusion of water $\left[= 79.6 \, {}^{Kcal}/_{Kg}\right]$
- C_{sa} : specific heat of water $\left[= 1 \, {}^{Kcal}/_{{}^\circ K \cdot Kg}\right]$
- T : air temperature
- T_0 : temperature of snowmelt [$=0$ °C]

4. Comparison between the tentative snow energy and the total available one

The tentative energy balance for the snow, computed at 273 °K considering the total available mass, is compared with the total available energy in order to decide if the snowpack is going to melt or not.

$$E^*_{t+\Delta t} \begin{cases} \leq C_{si}Z^*_{t+\Delta t}T_0 & \textit{the total energy is not enough for melting the snowpack} \\ > C_{si}Z^*_{t+\Delta t}T_0 & \textit{the total energy is enough for melting the snowpack} \end{cases}$$

5. Computation of the snowmelt produced by the excess energy

When the total energy is not enough to melt the snowpack, the water mass and energy budget are updated:

$$R_{sm} = 0$$
$$Z_{t+\Delta t} = Z^*_{t+\Delta t}$$
$$E_{t+\Delta t} = E^*_{t+\Delta t}$$

To the other hand, if the energy is sufficient to melt the snowpack, the amount of snow that is transformed into water (R_{sm}) is computed:

$$R_{sm} = \frac{E^*_{t+\Delta t} - C_{si} Z^*_{t+\Delta t} T_0}{C_{lf}} \tag{17}$$

$$Z_{t+\Delta t} = Z^*_{t+\Delta t} - R_{sm}$$

$$E_{t+\Delta t} = E^*_{t+\Delta t} - \left(C_{si} T_0 + C_{lf}\right) R_{sm}$$

4.6 PERCOLATION COMPONENT

For the deep aquifer flow the response time, caused by the vertical transport of water through the thick soil above this aquifer, is so large that horizontal flow in the aquifer can be assumed to be almost constant with no significant response on one specific storm event in a catchment (Todini E. , 1995). Nevertheless, the TOPKAPI model accounts for water percolation towards the deeper subsoil layers even though it does not contribute to the discharge, but simply as a lost outflow from the soil cell.

The percolation rate from the upper soil layer is assumed to increase as a function of the soil water content according to an experimentally determined power law (Clapp & Hornberger, 1978) but not to exceed the saturated soil hydraulic conductivity in the underlying deeper layer.

$$P_r = k_{sv} \left(\frac{v}{v_{sat}}\right)^{\alpha_P} \tag{18}$$

$$v_{sat}(\vartheta_s - \vartheta_r)LX \tag{19}$$

where:

- P_r : percolation [mm]
- k_{sv} : vertical soil saturated conductivity [m^3/s]
- v : volume [m^3]
- v_{sat} : local saturation volume [m^3]
- α_P : vertical non-linear reservoir exponent

α_P depending on the type of soil: may varies between 11, typical value for a sandy soil, and 25, typical for clay.

5. CASE STUDY: CATCHMENT DESCRIPTION

The chapter aims to describe the catchment physical characteristics looking for each component of the basin. A general overview of the geography, lithology and morphology, coupled with the meteorological considerations, is aimed to understand the hydrological behaviour of the catchment in order to better represent it with a mathematical model.

5.1 RENO CATCHMENT

Reno river is the tenth Italian river in terms of length (212 km) and basin extension (5040 km^2). These characteristics make him the major river, considering also the average discharge at the outlet, among those flowing into the Adriatic Sea on the south of the Po river. The majority of the basin is included in the Emilia-Romagna region (4467 km^2 hence the 88,4% of the whole Reno catchment). In Emilia-Romagna are incorporated the towns of Bologna (68,5%), Ravenna (17,7%), Modena (1,3%) and Ferrara (0.9%). Despite its huge dispersion in Emilia-Romagna, the Reno river originates in the Tuscany region: conventionally at the junction of two rivers (Reno di Prunetta and Reno di Campolungo) at 745 m a.s.l. The Tuscan territory within the catchment is 573 km^2 (11.6% of the whole basin) and are interested the towns of Florence (7.7%), Pistoia (3.1%) and Prato (0.8%) (Distretto Idrografico Appennino Settentrionale, 2010).

It is inhabited by nearly 2 million of peoples and includes areas with high concentration of industries (e.g. the metropolitan area of Bologna) and agricultural fields (e.g. area surrounding Lugo-Massa Lombarda for the production of fruit) (Fig.4 - source (Distretto Idrografico Appennino Settentrionale, 2010)).

The mountainous basin is extended for 2540 km^2, in this territory rainfall water flows on the mountain slopes converging into streams for all the drainage basin until the main river is shaped. Considering just this mountainous part of the catchment it measures 1061 km^2 with a maximum elevation of 1945 m a.s.l. and a minimum one of 60.35 m a.s.l. (at the gauge station at Casalecchio di Reno).

The mountain part of Reno catchment is composed by 8 principal rivers; 12 secondary rivers and 600 minor rivers.
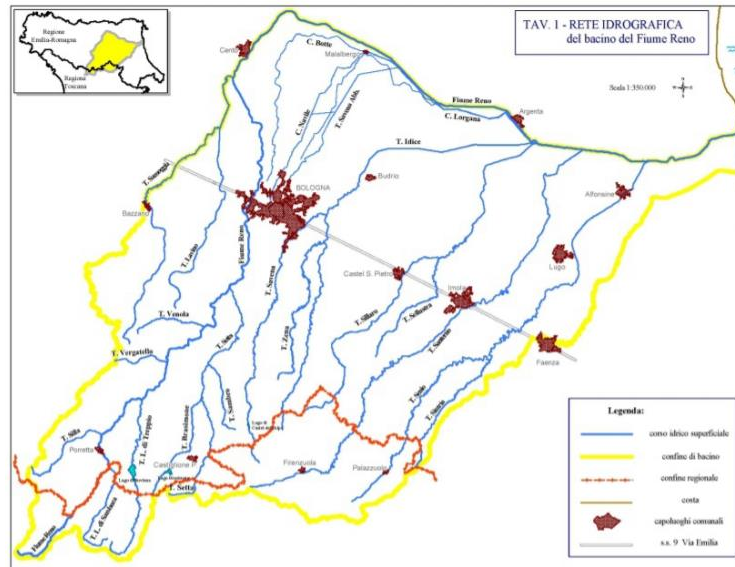
Fig.4 – hydrographic network and main urban settlements in the Reno catchment

As far as concerned the plain territories, the actual drainage basin of the Reno river is the result of different anthropogenic transformations, created for the purposes of hydraulic defence and reclaim of swamp areas in order to urbanize this plain part of the region. This historical evolution has determined among centuries a radical change in the territories between Bologna, Ferrara and Ravenna: the water streams which come from the Apennines and pass Via Emilia, flow within artificial embankment toward the Adriatic Sea for 124 km.

5.2 HYDROGRAPHY OF THE CATHCMENT

The catchment of the Apennines in the Bologna's area is mostly made of rivers originated in the Apennines' crest region, flowing until the end of the mountainous relief. They maintain an opposite direction with respect to the Apennines' one and being mostly parallel among themselves (Fig.5 - source (Wikipedia, 2019)).
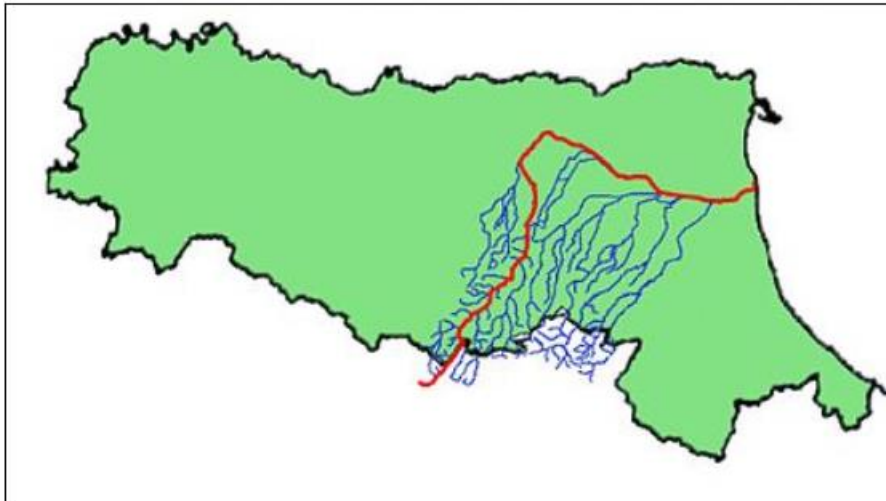
Fig. 5 – Hydrography of the Reno catchment

The rivers in this area are characterized by a torrential stream with peak flows in the period between late Autumn, Winter and early Spring (in particular December, February and March). This discharge value is much higher, even double, compared with the summer months. The reason is the type of alimentation which is almost entirely given by rainfall; just a minor part is composed by the superficial water equivalent made by the snow melt. Nevertheless, the dominant impermeable nature of soils is the reason of the balance between outflows and inflows, but there are some exceptions. For instance, in September is measured the minimum runoff coefficient value (0.16) because of the water losses given by dry soils presence, which are typical of the autumnal dry weather and the hot one in summer. Therefore, the discharge peak value is not measured in correspondence of the maximum outflow (in November) but later, in March, because of the water contribution from the snow melt.

5.3 RIVER CLASSIFICATION

All Reno's tributaries are characterized by a recognisable catchment individuality. Is possible to identify a main catchment, 5 other sub-basins and other smaller rivers, all part of the Reno's catchment (Fig.6 - source (Barbieri, s.d.)). Rivers are classified on the basis of the sub-basin extension, indeed to this

size is related the average maximum discharge value. The classification can be summarized as follow:

- **Principal rivers**: the ones with a catchment grater or equal to 40 km^2
- **Secondary rivers**: the ones with a catchment in between 40 and 13 km^2.
- **Minor rivers**: all those streams which are not included in the previous classification, showed in the Technical Regional Cartography with a scale of 1:5000.
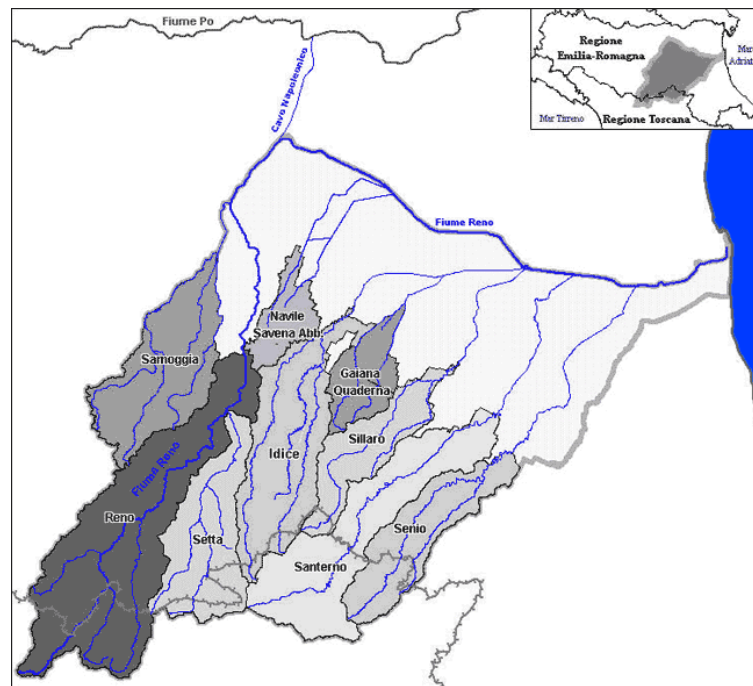
Fig.6 – sub-basin identification within the Reno catchment

5.4 GEOMORPHOLOGICAL ASSET

According to lithological, stratigraphic, structural and morphological characteristics, it is possible to subdivide the Reno catchment in 5 sectors:

- **Apennine Ridge**: in correspondence of the Tyrrhenian-Adriatic watershed is made by turbidite sedimentary deposits, arenaceous-pelitic rocks characterized by a quartzous-feldspathic composition, with schistic-clayey-marly base and interposition of sandstones and limestones. The landscape is characterized by deep torrential furrows and

31

rocky outcrops coming out from the cliffs. Here are localized the upper part of the principal drainage basins.

- **Apennine of Emilia**: the is the mid-west portion of the Reno catchment. Is the area mostly interested by deformations which cause high slope instability (because of the low mechanical properties of the outcrop rocks). Is characterized by sedimentary rocks composed by a chaotic structure of clay and limestones with inclusions of sandstone. Hence, landslides are caused by mud flows which may interrupt river paths causing their deviation and the erosion of embankments. There are also others rock formations like the so-called "Ligurian Flish" (a turbidite sequence of marly-limestone rocks and arenaceous-pelitic formations) and "Epiligure Sequence" (marlstones of different colours and quartzous-feldspathic sandstones). The poor mechanic characteristics of these rocks interest both the superficial layer and the substrate giving to the slopes a characteristic corrugated shape with concavities and convexities.

- **Lower Apennine**: defines the northern mountainous part of the catchment arriving until the lowland. Is characterized by modest heights and high geomorphological dynamicity (due to the low resistance of outcropping rocks). In correspondence of the main rivers there are large terraced surfaces typical of the landscapes like Badlands (Calanchi) and karst regions.

- **Apennine of Romagna**: the east-side part of the catchment, defined by arenaceous-pelitic deposits originating in the Alpes. In general, this sector is less tectonically deformed with respect the previous ones and landslides are made mostly by rocks (rarely by mud) in correspondence of the principal tectonic structures.

- **Lowland**: from the Apennines boundary until the Adriatic Sea, it is part of the Pianura Padana. The actual conformation of the latter is given by climate changes caused by the last ice age of roughly 10.000 years ago and the consequent sea level fall shaping the current coast line. At the

basis of its origins there was two different lithological processes: the alluvial plain and the river delta plain.

Therefore, an overall panoramic of the morphology depicts the upstream part of the catchment (a third of the whole basin) made of resistant limestones and sandstones. This relatively easy erodible part represents the sub-Ligurian folded rock units (nappes), that have been exposed by erosion and removal of the Ligurian cover-rock. Surface mechanisms in this area consist of debris flow and mass wasting of Pleistocene glacial deposits. On the contrary the downstream two-thirds of the catchment consist on relatively thin Pliocene-aged sandstones acting like a caprock for the wide spread marls, mudstones, siltstones and silty sandstones typical of the Ligurian and Epiligurian units. Because of the impermeable and erodible characteristics of these rocks, in addition to the heavy rainfall periods on which this area is subjected, this part of the catchment is marked by Badlands (Calanchi), originated from runoff processes, causing soil erosion and landslides. In conclusion the morphology of this areas differs among steep slopes covered by woods and low hills with grasslands.

5.5 HYDROLOGIC ASSET

Given the impermeable characteristics of the lithological structure of the catchment, all the rivers in the mountainous area are defined by a torrential stream. As a consequence, the trend of discharges in the basin reflects the one of precipitations, with some exceptions in winter and spring due to snow melt. The average annual discharge for the Reno varies between 15 to 26 L/sec (Reno, 2002). At the gate station of Casalecchio di Reno the average annual discharge is 26 m^3/s, instead at the outlet of Casalborsetti is 95 m^3/s. The average measured value for flooding events is just barely above 1000 m^3/s, usually registered in March. Minimum values are 4 m^3/s at Casalecchio and 0.6 m^3/s at Casalborsetti, even if less than a century ago the minimum discharge was never less than 5 or 6 m^3/s. The latter datum depicts that the river, especially in mountainous areas, is strongly exploited among years for human purposes (domestic and irrigation). The hydrography of the catchment was altered by the construction, on the

tributaries of the main stream of the Reno river, of five large hydroelectric dams (Suviana, Brasimone, Pavana, Santa Maria and Molino del Pallone) with a total capacity of 52×10^6 m³. Almost all the reservoirs are linked together by underground channels.

5.6 LAND USE

Land cover of the catchment is dominated by woods. This is the result of the reforestation operations started in the 1950s and proceeding nowadays as a consequence of mountain areas abandonment. The result is that the wood percentage has increased from 24% to 60% in between 500 m to 900 m a.s.l. and from 70% to 98% above 900 m a.s.l. The upper part of the catchment is mainly covered by chestnuts, oaks and beeches, while hillsides are characterized by coppices, pastures (especially at higher altitudes), shrubs and crops. Regarding the agricultural landscape the post-war scenario defines the abandonment on mountainous areas. In fact, the technological agricultural improvements lead to prefer flat fields (Pianura Padana) with respect to mountainous cultivated areas, which face a reduction from almost 40% to 5% (D.Pavelli, 2013). The valley is covered by crops, vineyards, orchards and urban areas.

5.7 CLIMATIC CLASSIFICATION

Falling within the Apennine climatic zone, the Reno catchment is characterized by two periods of high precipitations (autumn and spring) and one period of low precipitations (summer) when, between June and August, a long dry season persists. The average annual precipitation measured on a date set of 81 years (D.Pavelli, 2013) from 1926 to 2006, is 1307 mm/year. Regarding the seasonal values, the mean precipitation is 355 mm in winter (December, January and February), 322.2 mm in spring (March, April and May), 194.0 mm in summer (June, July, and August) and 434.4 mm in autumn (September, October and November). From November to March, in the higher catchment areas, some snowfalls may occur.

6. CASE STUDY: MODEL CALIBRATION

The study defines the reliability of the model working with forecasting data in different scenarios: firstly, under some assumptions of predicted rainfall based on the observed one, then using forecasting data of precipitation in a real-time configuration. In order to do that, it is necessary to estimate the reliability of the spatial distribution of the rainfall with an analysis of spatial variability. Most importantly, the model needs to be calibrated and validated on a chosen period.

As the Reno river has a torrential character at Casalecchio cross section, the simulations described here below consider only the upper part of the basin, which for sake of simplicity, from now on, will be called "Upper Reno catchment".

6.1 PARAMETER REQUIREMENTS

The methodology to derive parameters for the TOPKAPI model from the Reno catchment information is based essentially on two main procedures:

- Determination of the catchment geometrical characteristics: the grid cell size, the cells composing the river network and how the cells are connected.
- Assignment of the parameter values that better represent the physical behaviour of the catchment.

Determination of geometrical information

As already stated in the previous chapter, the model requires the definition of a grid that divides the catchment space into squared cells that must be connected in order to model the surface and subsurface flows within the catchment. Therefore, the grid lateral dimension (X value in the model equations) is imposed with a resolution of 500m and the drainage network is defined by choosing the 8-direction scheme. At this point, using the DEM (Digital Elevation Model) file of the catchment it is possible to determine the outflow direction of each cell, and thus the direction of the steepest outflow path from an active cell to the neighbouring downstream cells. In particular, the method identifies the steepest

downslope flow path among each cell of a raster DEM and its eight neighbors, and defines this path as the only flow path leaving the raster cell. The final step to define the drainage network is selecting a threshold catchment area at the bottom of which a source channel originates; all cells with a catchment area greater than this threshold are classified as part of the drainage network. The threshold value chosen for the area is fixed at 0.25 km^2. In reality, the extension of the drainage network changes within the season and depending on the flow intensities, but this value is considered to be an acceptable compromise. In fact, the value of 0.25 km^2 is in accordance with Todini's recommendation that the ratio between the number of channel cells and the total cells number should be a value ranging between 5% and 15% of the total catchment area (Todini, 1996). The drainage network is finally defined.

Physical model parameters

One of the advantages of the TOPKAPI model is its physical basis that allows the link between model parameters and catchment characteristics. All the parameters values, or range of values, used in this study are reported in the Table 2 as well as the references from where the values are taken.

The constant parameters (X,A$_{threshold}$) are assigned, as already noted in the previous section, as well as the 0.5 value fixed for the flow partition coefficient (F_P) to split the overall cell outflow (overland + soil) into the channel contribution and the next downstrem soil contribution.

The slopes of the ground $\tan(\beta)$ (β_1 and β_2 for the drainage coefficient) are directly computed from the cell elevation of the DEM, as well as the values for the angle riverbed $\tan(\gamma)$ and the slopes used to transfer the flow in the channel drainage network $\tan(\beta_C)$.

For the soil cell-specific parameters the soil map is mainly used to derive the values for the residual and saturated soil moisture content (θ_r, θ_s), the soil depth of the cell (L), the horizontal and vertical permeability (K_s, K_{sv}) and the vertical non-linear reservoir exponent for percolation (α_P). The pore-size distribution parameter for the horizontal flow in the soil cell is uniformly set to the value 2.5

(Liu & Todini, 2002). The ordering method of Strahler (1957) is used to infer the values of channel roughness Manning's coefficients (n_C). In Liu and Todini (2002), channel orders of 1,2,3 and 4 are assigned with the respectively values 0.045, 0.04, 0.035 and 0.035 for the same Reno catchment. The overland roughness Manning's coefficient (n_o) is derived from the land use map as well as the value for the crop factor K_C.

6.2 DATA REQUIREMENTS

In order to define the morphological, physical and hydraulic characteristics of the basin, Tab.3 defines the maps used in the study and their references. Data concerning rain, temperature and discharge are given by regional agency ARPAE of Bologna and cover entirely the period from the beginning of 2005 to the end of 2013. A summary of gauges information is following given in Tab.4.

	Precipitation	Temperature	Discharge
Source	ARPAE Emilia-Romagna	ARPAE Emilia-Romagna	ARPAE Emilia-Romagna
Period	01/01/2005 – 31/07/2013	01/01/2005 – 31/07/2013	01/01/2005 – 29/01/2014
Time Step	1 hour	1 hour	1 hour
Stations number	109	56	18
Stations spacial distribution			
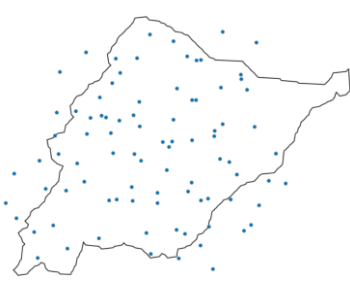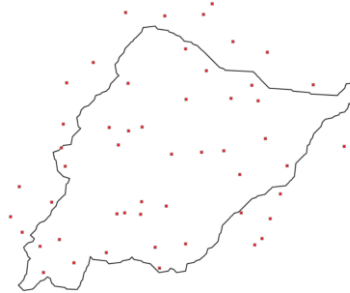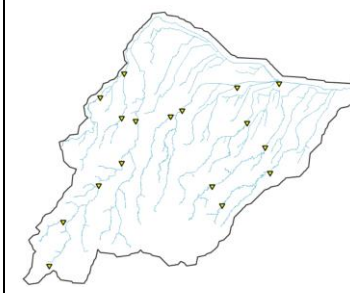
Tab.3 – data information concerning precipitation, temperature and discharge

37

Tab.2 – Value of TOPKAPI model parameters

		Parameters	Values	Origin and References
Constant values	X	Lateral dimension of the cell grid [m]	500	
	$A_{threshold}$	Threshold catchment area [km^2]	0.25	
	F_P	Flow Partition Coefficient	0.5	[0.0 – 1.0]
Soil	θ_r	Residual soil moisture content	0.004 – 0.1005	Soil Map
	θ_s	Saturated soil moisture content	0.3791 – 0.4973	Soil Map
	L	Soil depth [m]	0.3 – 2.72	Soil Map
	α_S	Horizontal non-linear reservoir exponent	2.5	Liu and Todini (2002)
	K_S	Horizontal Permeability at Saturation [m/s]	9.9E-007 – 1.32E-003	Soil Map
Overland	n_o	Manning's overland roughness coeff. [m$^{-1/3}$s^{-1}]	0.03 – 0.28	Landuse Map
Channel	n_C	Manning's channel roughness coeff. [m$^{-1/3}$s^{-1}]	0.02 – 0.075	Strahler's order method
ET	K_C	Crop Factor	0.2 – 1.25	Landuse Map
Snowmelt	T_S	threshold Temperature for snowfall / rainfall	0°C	
	Albedo	Albedo or reflection coefficient	0.4	[0.0 – 1.0]
Percolation	K_{SV}	Vertical Pemeability at Saturation [m/s]	9.9E-10 – 1E-07	Soil Map
	α_P	Vertical non-linear reservoir exponent	11 – 25.38	Soil Map

Tab.4 – input maps for the TOPKAPI model

Category	Web Source	Description	
DEM	http://srtm.csi.cgiar.org	It's been used a DEM with a resolution of 90m derived from the data of USGS/NASA SRTM mission (Jarvis, Reuter, Nelson, & Guevara, 2008)	
Soil Type	Emilia-Romagna: http://geo.regione.emilia-romagna.it/cartpedo/index.jsp?liv=3	1:250.000 scale map, 1994 (updated in 2000) made by servizio Pedologico della Regione Emilia Romagna	
	Tuscany: http://sit.lamma.rete.toscana.it/websuoli/	1:250.000 scale map	
	The two maps are merged togheter with the MapWindow GIS tool		
Land Use	http://www.eea.europa.eu/data-and-maps/data/corine-land-cover-2006-raster-3#tab-gis-data	Corine Land Cover 2006 raster data Version 17 (12/2013), with resolution of 100m	
Hydrography	http://www.fao.org/geonetwork/srv/en/main.home	FAO Geo Network	
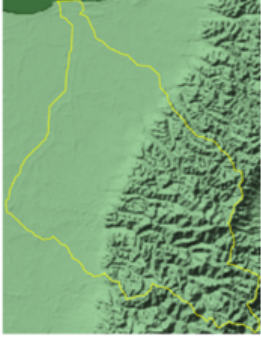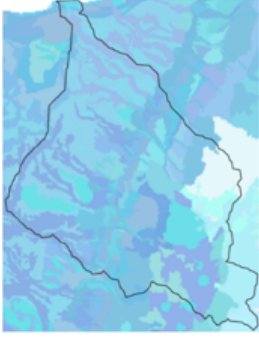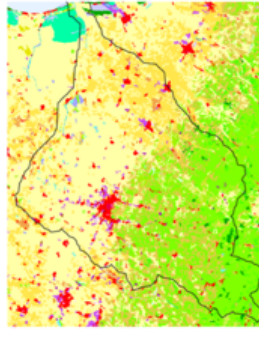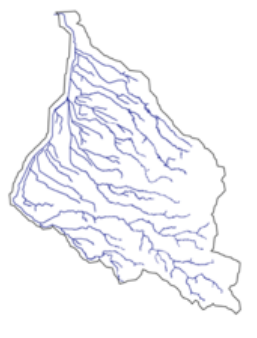
6.3 MODEL CALIBRATION

6.3.1 Definition of the simulation period

The model calibration is performed at 1-hour time-step using the hydrological dataset of 2012-2013. The latter is selected for the calibration in the Upper Reno river basin (considering Casalecchio as the final output of the catchment), since in the period from 18 to 19 march 2013, a relatively large flood events occurred with a peak discharge of 1168 m^3/s. The choice to consider a set of data covering 9 months is related to the "**warm-up period**" needed from the model for the automatic calibration of average soil moisture and river level/width value parameters. In fact, the model assigns given initial values (varying from 0 to 1) for the latter parameters according to the seasonality and it requires to be run over a period of some months in order to find the better values to simulate, in the best way, the events we are interested in. In order to understand the influence of the warm-up period, Fig.7 compares the result of the simulation over the full 9-month period (on the Upper Reno catchment) with the one which does not consider the initial warm-up period from October to February. Firstly, the dispersion diagram compared with the 1-1 line shows clearly how the results obtained in the initial months of the simulation (October and November) are the most distant from the bisect line of the plot, which means high error in the simulated discharge with respect the observed one. On the contrary, the results tend to coincide with the 1-1 line in the latest months of the warm up period.

It is important to take into account the influence of the warm-up period in the overall judgment of the result goodness, and this is evident in the comparison between the regression line obtained considering the overall set of results covering 9 month of simulation (inclusive of warm-up period) and the one obtained, instead, neglecting the first 5 month. The latter tends to better replay the ideal 1-1 line and this demonstrates how the warm up period is necessary in order to partially auto-calibrate the model and simulate in the best condition the catchment hydrologic response in the last part of the simulation.
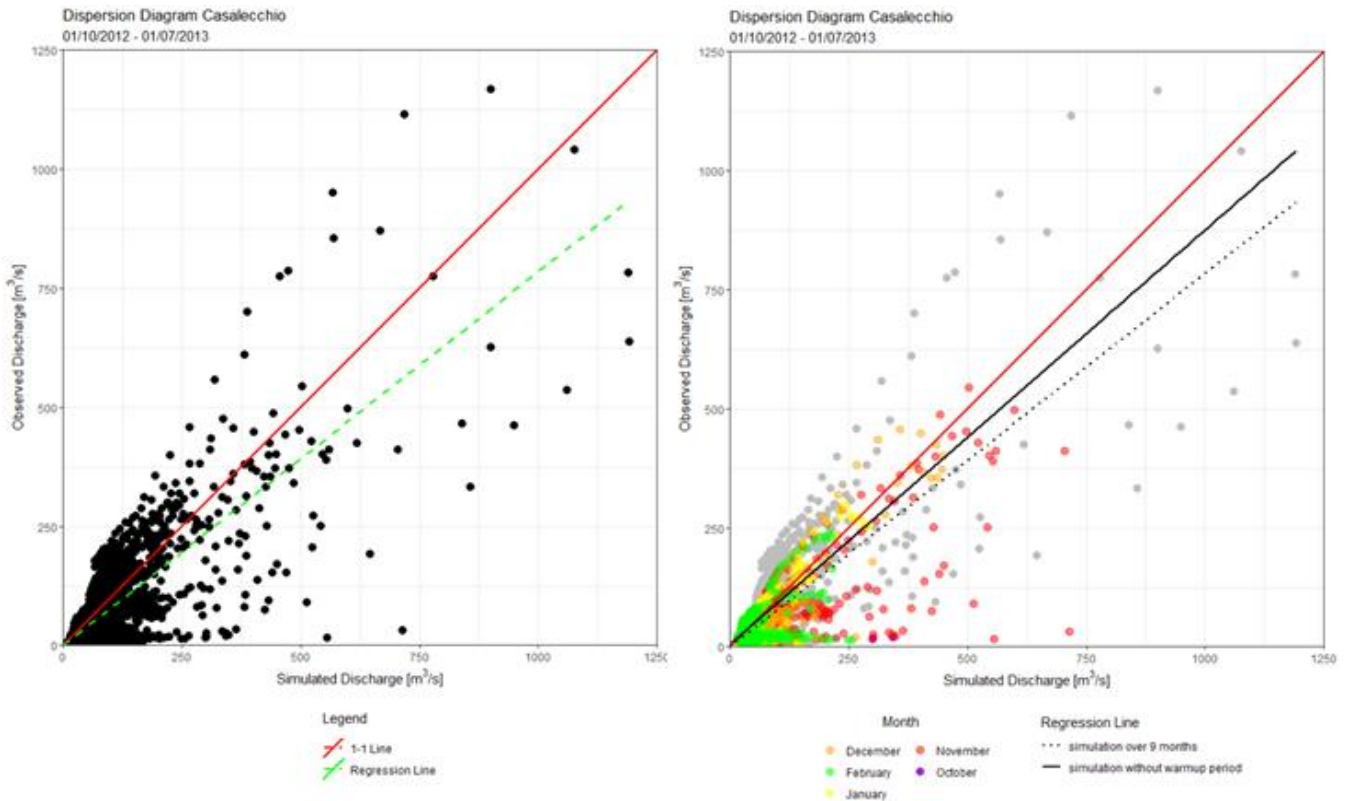
Fig.7 – Comparison between the general dispersion diagram of the full 9-month simulation period (upper plot) and the one where is underlined the impact of the warm-up period from October to February (bottom plot)

6.3.2 Parameters calibration

Given its physically-based nature, the model is subjected to several uncertainties associated with data on:

- The information on topography, soil characteristics and land cover;
- The approximate methods and tables used to infer physical parameters from the data;
- The approximations introduced by the scale of parameters representations.

For these reasons the calibration of parameters is necessary but, as suggested from Liu and Todini (2002), it is more related to an "adjustment procedure" that can be achieved through a simple trial-and-error method. In the present study the

initial parameters are provided by Progea srl on the basis of the application of TOPKAPI 4-direction scheme on the same basin for the year 2015.

Just few small adjustments are sufficient to calibrate the model with satisfactory results. In particular, the parameters which most influence the hydrological response of the basin are the ones which describe the water behaviour in the main components of the model:

- Soil depth (L) and horizontal vertical permeability at saturation (K_S) for the soil component
- Manning's roughness coefficients for overland and channel components (n_o, n_C)
- Crop factor (K_C) for the evapo-transpiration component
- Threshold temperature (T_S) for the snowmelt component
- Vertical permeability at saturation (K_{SV}) for the percolation component

Giving the high complexity in calibrating the parameters that characterize the overland and channel behaviour without the use of automatic methods, the value of the Manning's roughness coefficient is considered the same of the ones already calibrated from Progea in their study. Furthermore, considering the Apennine climate conditions, it is reasonable to fix the threshold temperature for snow/rainfall boundary to 0°C without a particular calibration procedure. The crop factor coefficient is maintained the same of the tabular values without a particular calibration. In fact, the initial calibration tests demonstrate that the parameters which most affect the results of the simulation are the ones connected to the soil and percolation components. This means that the manual calibration procedure is limited to the adjustment of just three parameters: L, K_S and K_{SV} which define the behaviour of the water in the passage from a cell to the next one. In particular, a high value of K_S means more water able to move in the downward direction and, therefore, more water considered in the overall discharge in the basin. On the contrary, a low value of horizontal permeability means that the water within soil cell faces a tendency to be stucked in it, reducing the basin discharge and increasing the evapotranspiration value of the catchment. The same mechanism is at the basis of the vertical permeability value calibration:

the higher is the value of K_{SV}, the more is the amout of water which is considered lost by the model because of percolation in the deep layers. The manipulation of this value it's useful in cases where the difference between the simulated discharge and the observed one may be corrected by simply adding or losing discharge from the model. Finally, the value for the soil depth is modified, where necessary, on the basis of the soil list information taken from Regional Emilia-Romagna Soil Legend (Romagna, s.d.).

The methodology chosen to calibrate the parameters is aimed to separate initially each sub-basin making part of the Upper Reno catchment and define the soil mostly present for each sub-basin. Then, proceeding from top to bottom, the upper sub-basin (Pracchia) is firstly considered when the parameters of the most present soil types (PON1_MRS1_PGG1) are calibrated. Analogously, the downward sub-basin of Silla first (modifying 6Ba and 7Ba soil parameters) and Vergato then (MNT1_GIU1_GSP1) are calibrated. Finally, by calibrating the remaining soils of the Casalecchio basin, the total Upper Reno catchment is calibrated. A more specific description of the results is given in the next section of the chapter. Adjustment of parameters was performed manually and, at the end, the values given in Table 5 are retained.

In order to properly calibrate the model, it is necessary to consider some soils separately. In particular, for those soils which are present either in the Reno basin and in the Setta one (e.g. 6Ba, 6Ca, 6Fe, 7Ba, PON1_MRS1_PGG1) a second identification code is manually created: the "old" code (e.g. 61 for the 6Ba soil) is preserved for those soils present in the Setta basin, instead the "new" code (e.g. 1061 for the same 6Ba) identifies soils within the Reno basin only. According to this expedient, it is possible to calibrate the soil parameters of the two basins separately. The reason is that the convergence of the Setta river in the Reno one (after Vergato) may get problems in the model simulation if the two basin-physical properties are considered equal. Indeed, despite the fact that the two catchments share the same lithology, soils belong to morphologies evolved from two different rivers and so also the physical properties may be different. The Fig.8 shows an example of separation of a soil present in both the basins.

Tab.5 – Calibration of parameters

Name	Description	cell_ID		K_s Horizontal permeability	L Soil depth	K_{sv} Vertical permeability
5Df	Low Apennines soil. Moderately steep with 10%-30% slope with mixed composition of alkalized limestones	52	from		1.55	
			to		0.5	
5Dg	Low Apennines soil. Moderately steep with 12%-25% slope with mixed composition of alkalized limestones	53	from		0.98	
			to		0.3	
6Ba	Middle Apennines soil. Wavy and moderately steep with 8%-20% slope, very deep and with mixed composition of alkalized limestones	61	from	9.90E-07	1.43	9.90E-10
			to	9.90E-07	0.4	9.90E-10
		1061		9.90E-05	1.43	9.90E-08
6Ca	Middle Apennines soil. Moderately steep, very deep, mixed limestone composition characterized by shingles	63	from	1.45E-06	0.99	1.45E-09
			to	1.45E-07	0.3	1.45E-10
		1063		1.45E-04	0.99	1.45E-07
6Fe	Middle Apennines soil. Wavy and moderately steep, very deep and with mixed composition of sour and weakly alkalized limestones on the surface	77	from	1.13E-06	1.44	1.13E-09
			to	1.13E-07	0.7	1.13E-10
		1077		1.13E-04	1.44	1.13E-07
7Ba	High Apennines soil. Highly steep with more 50%-70% slope. Rocky, stony with mixed composition (not limestones)	84	from	4.57E-06	0.95	4.57E-09
			to	4.57E-07	0.5	4.57E-10
		1084		4.57E-04	0.95	4.57E-08
7Da	High Apennines soil. Highly steep with 25%-80% slope. Rocky, stony with mixed composition characterized by shingles	91	from	2.93E-06		2.93E-09
			to	2.93E-04		2.93E-07
PON1 MRS1 PGG1	Very deep hillsides made of felpspathic-quartzous sandstone with intercalation of marls and shales	302	from	2.93E-06		2.93E-09
			to	1.32E-03		2.93E-07
		1302		1.70E-03		2.93E-07
MNT1 GIU1 GSP1	Very deep hillsides made of silty shales, marls, mudstones and turbidite limestones	305	from	3.77E-06	0.75	3.77E-09
			to	3.77E-05	0.3	3.77E-10
		1305		3.77E-03	0.75	3.77E-08
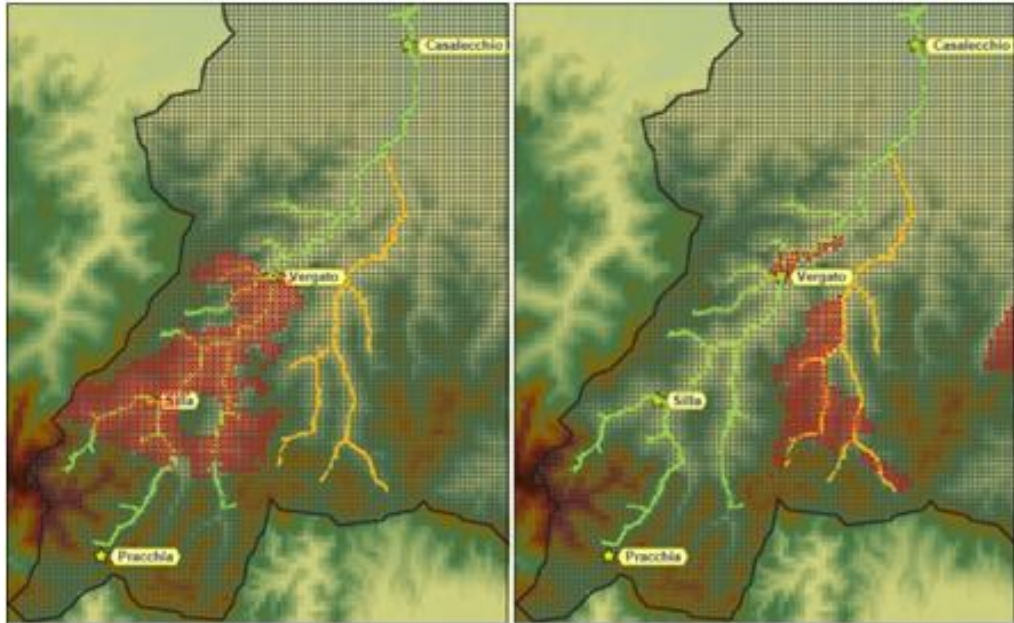
Fig.8 – Separation of the type soil 6Ba between the basins of the Reno river (on the left) and the Silla river (on the right) for the purpose of calibration

6.3.3 Results of the calibration

The following results are showed in order of calibration, in a top-to-bottom direction starting from the most elevated Pracchia sub-basin. The calibration proceeds with the analysis of the results obtained for the Silla, Vergato and finally for Casalecchio.

The figures below, depending on the considered sub-basin, summarize the results of the simulation with two hydrographs (one for the whole simulation period, comprehensive of warm-up period, and one for the main event/s within it) and a dispersion diagram, in order to better visually compare the observed discharge with the simulated one by using both the regression line and the ideal 1-1 line (ideal case in which the discharge simulated is perfectly the same of the observed one). Moreover, a picture of the sub-basin helps to understand which part of the general catchment we are considering.

The results concerning the upper sub-basins with respect to the final outlet of Casalecchio show a tendency of the model to underestimate the value of the simulated discharge compared to the observed one. This is what emerges from the dispersion diagrams of Pracchia, Silla and Vergato but, taking a look at the hydrograph of the whole simulation period (9-months), it is possible to understand that the reason of this model behaviour is typical of the warm-up period characterizing the first months of the simulation (usually 5 or 6). In fact, looking at the period of the simulation in which we are most interested, hence the last winter-initial spring period, the model simulates the observed discharge with good results for all sub-basins. The same behaviour is reflected also in the bigger sub-basin of Casalecchio which contains all the previous.

Giving these observations, the obtained set up of parameters and the choice of a simulation period of at least 9 months is taken also for the further tests of spatial variability, out of sample simulations and real time forecasting.
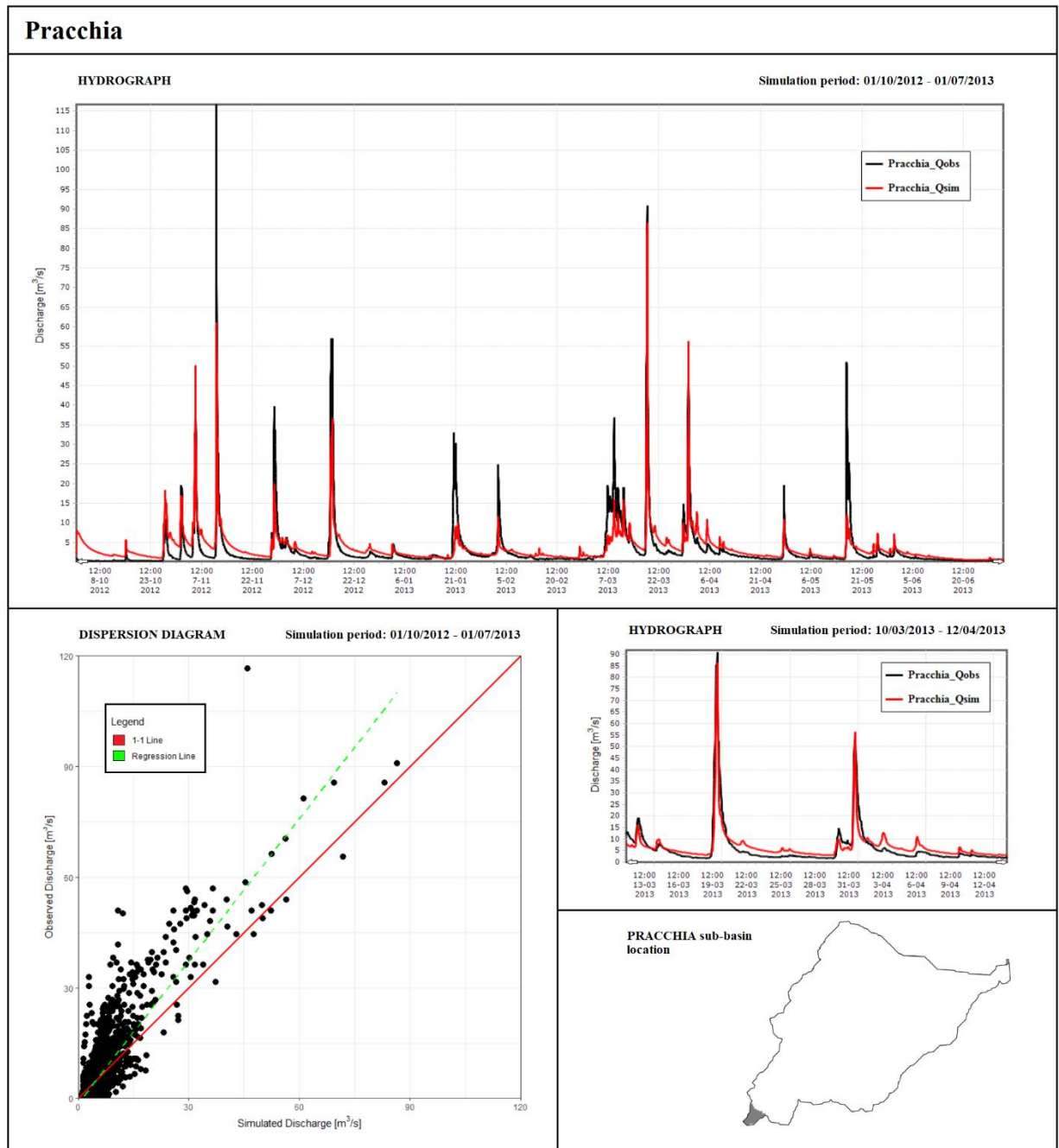
Fig.9 – Simulation results concerning the output Pracchia
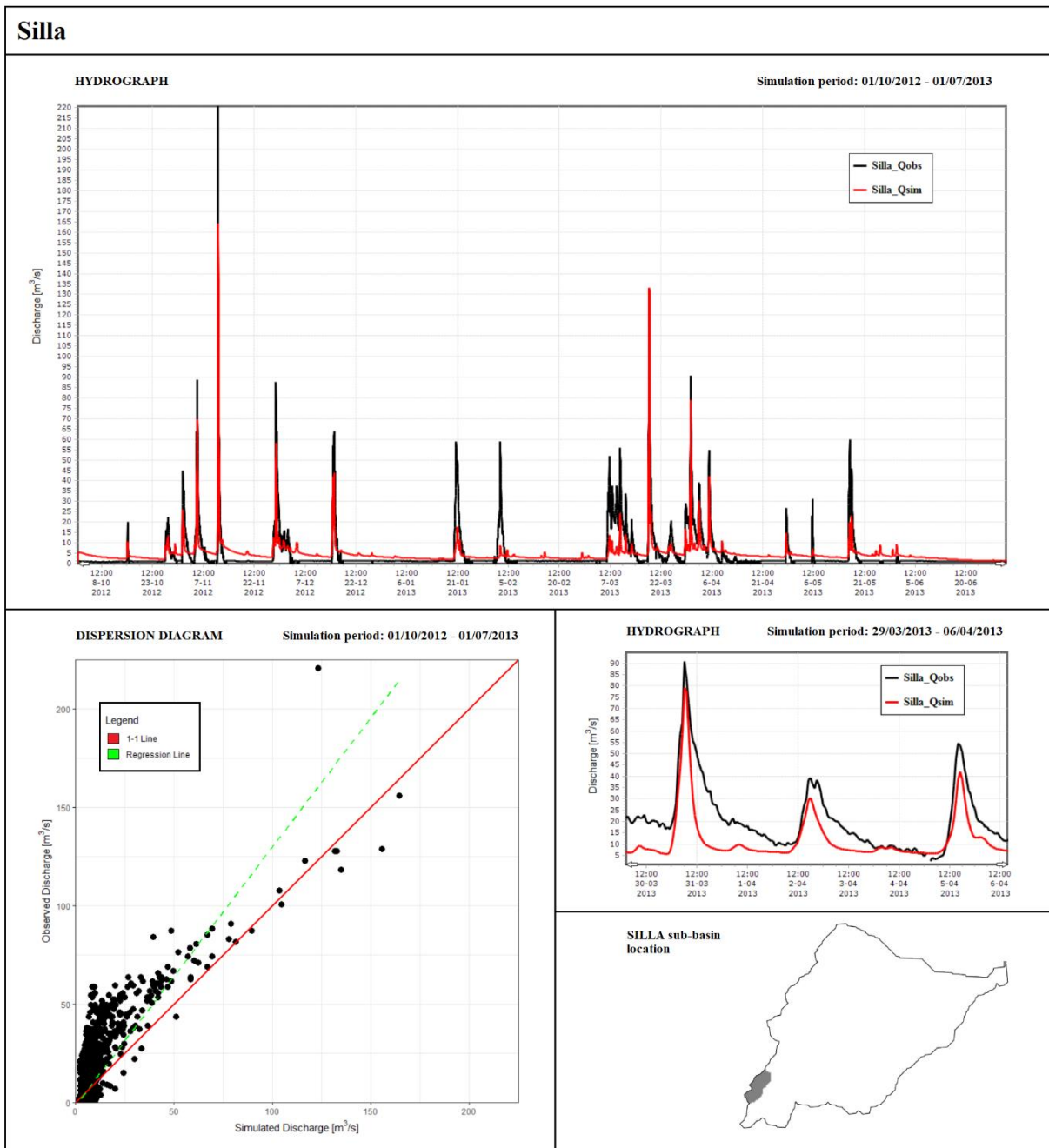
Fig.10 – Simulation results concerning the output Silla
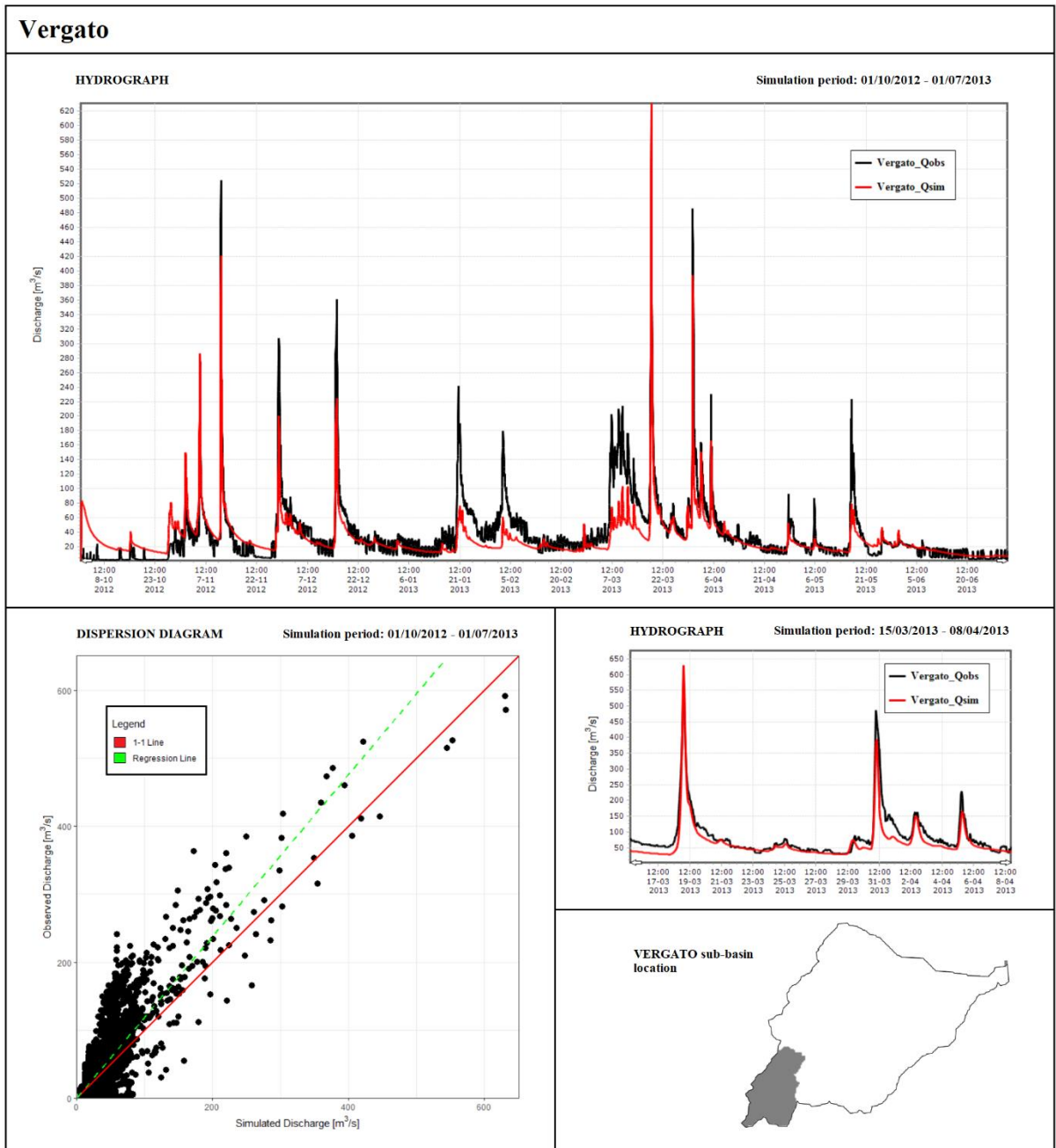
Fig.11 – Simulation results concerning the output Vergato
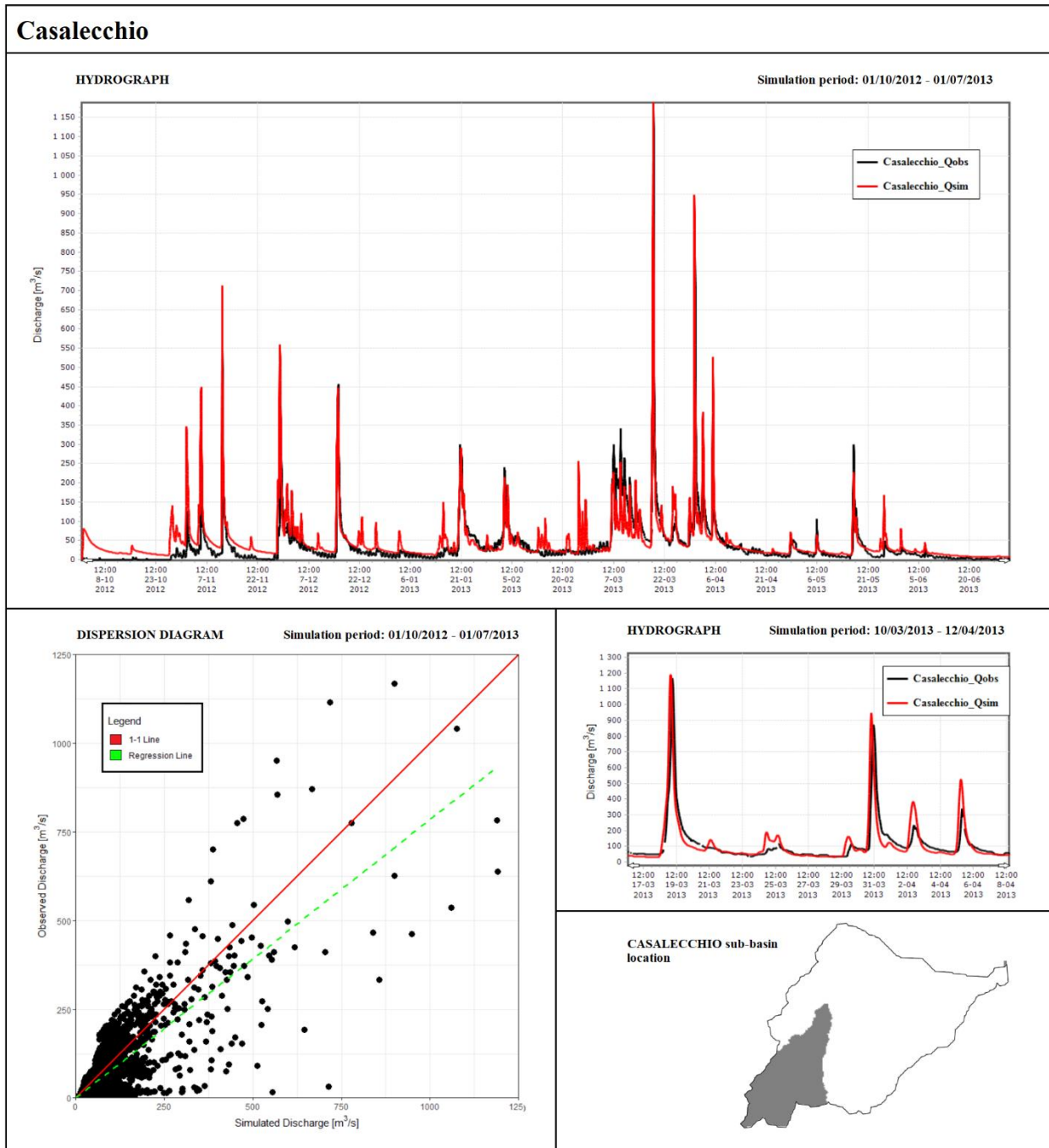
Fig.12 – Simulation results concerning the output Casalecchio

6.4 MODEL VALIDATION

In order to validate the model, the simulation is applied to different periods. In particular among the overall available data sets from 2005 to 2013, the second and the third events in terms of higher discharge measured are selected. Therefore, the model is applied both to the period between 2009 and 2010 and between 2008 and 2009 (Fig.13).

The goodness of results is evaluated by comparing the simulated discharge and the observed one with the use of a dispersion diagram, where the vicinity of scatter dots with the red highlighted line helps to understand the general difference among simulated versus observed discharge. For the same purpose the green dotted regression line shows the difference with the red line observation=simulation. Both simulations indicate how such calibration seems to provide a reliable discharge modelling.
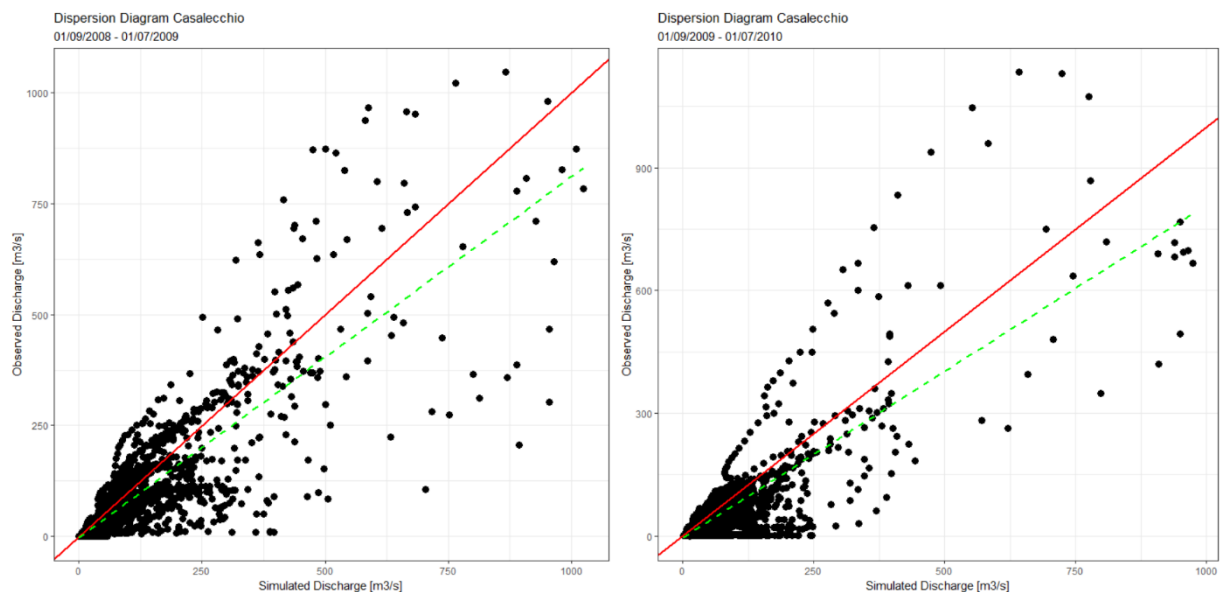
Fig.13 – Dispersion diagrams for the results of the simulations in between 2008-2009 and 2009-2010

7. CASE STUDY: MODEL IMPLEMENTATION

7.1 ANALYSIS OF SPATIAL VARIABILITY

A key issue in rainfall-runoff modelling is to assess the importance of the spatial representation of rainfall on streamflow generation. Moreover, concerning small (<100 km^2) and medium to large (100-2000 km^2) catchments like the Reno one, the spatial resolution of rainfall is one of the most important factors that must be taken into account (Arnaud, Bouvier, Cisneros, & Dominguez, 2002). In fact, studies show that as the scale increases, the catchment response time distribution becomes the dominant factor governing the runoff generation (Bell & Moore, 2000). On the other hand, it is important to recognize that the spatial variability of rainfall is often identified as the major source of error in investigations of rainfall-runoff processes and hydrological modelling (O'Loughlin, Huber, & Chocat, 1996) and in addition, for small catchments, the spatial variability of precipitation can be very strong (Woods, 2000).

Distributed models such as TOPKAPI have the potential to represent the effects of spatially variable inputs like rainfall, making them an appropriate tool to investigate the role of spatial rainfall on runoff. In particular, the spatial variability of the rainfall within the catchment is considered performing two simulation with a different distribution of rain gauges within the basin itself. It is important to specify that, also in this phase of the test, only the result for the Casalecchio outlet is considered. Therefore, the spatial variability of rain gauges is considered just within the borders of the Upper Reno catchment.

The following two tests on the spatial variability may be summarized as:

- **Test1**: the rainfall event is uniformly spread over all the rain gauges within the catchment. In order to do that, the rainfall amount per hour measured from each rain gauge is substituted with the average value among all the data set for the same hour.

- **Test2**: the rainfall event is concentrated in the middle of the basin. In order to do that, only the rain gauge of Vergato like input of precipitation is considered.

The results of Test1 (Fig.14) show that the model, under the hypothesis of uniform rain events, returns a good response in terms of simulated discharge. Indeed, both the illustrated hydrographs (one for the whole simulation period which includes the initial warm-up period, and one picturing the main event) show a good correspondence between the simulated and the observed discharge. In addition, the dispersion diagram depicts firstly the results with respect to the 1-1 line (observed discharge=simulated discharge), and then it compares the spatial variability results with the ones obtained with the simulation which takes into account the original full set of rain gauges. With this latter comparison it is possible to observe a negligible difference between the two simulations. This demonstrates the good response of the model using an average value of rain obtained from a spatial distribution of rain gauges in high-resolution.

The results of Test2 (Fig.15), on the other hand, depict a general underestimation of the model simulation of the discharge at Casalecchio demonstrating that the hypothesis to consider just the rain in the middle of the catchment is too restrictive.
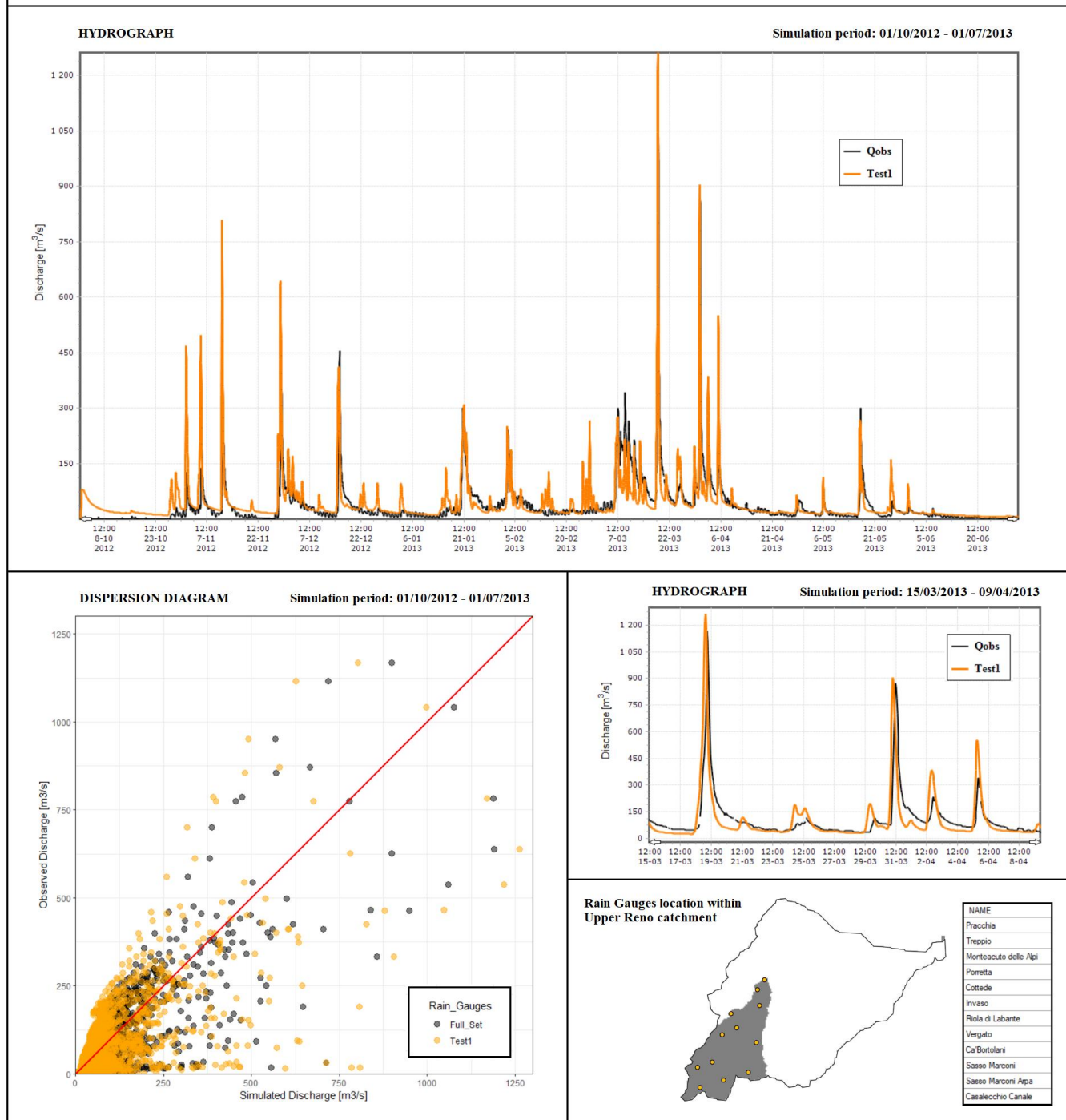
Fig.14 – Results on Test1 concerning rain gauges spatial variability within the Upper
Reno catchment
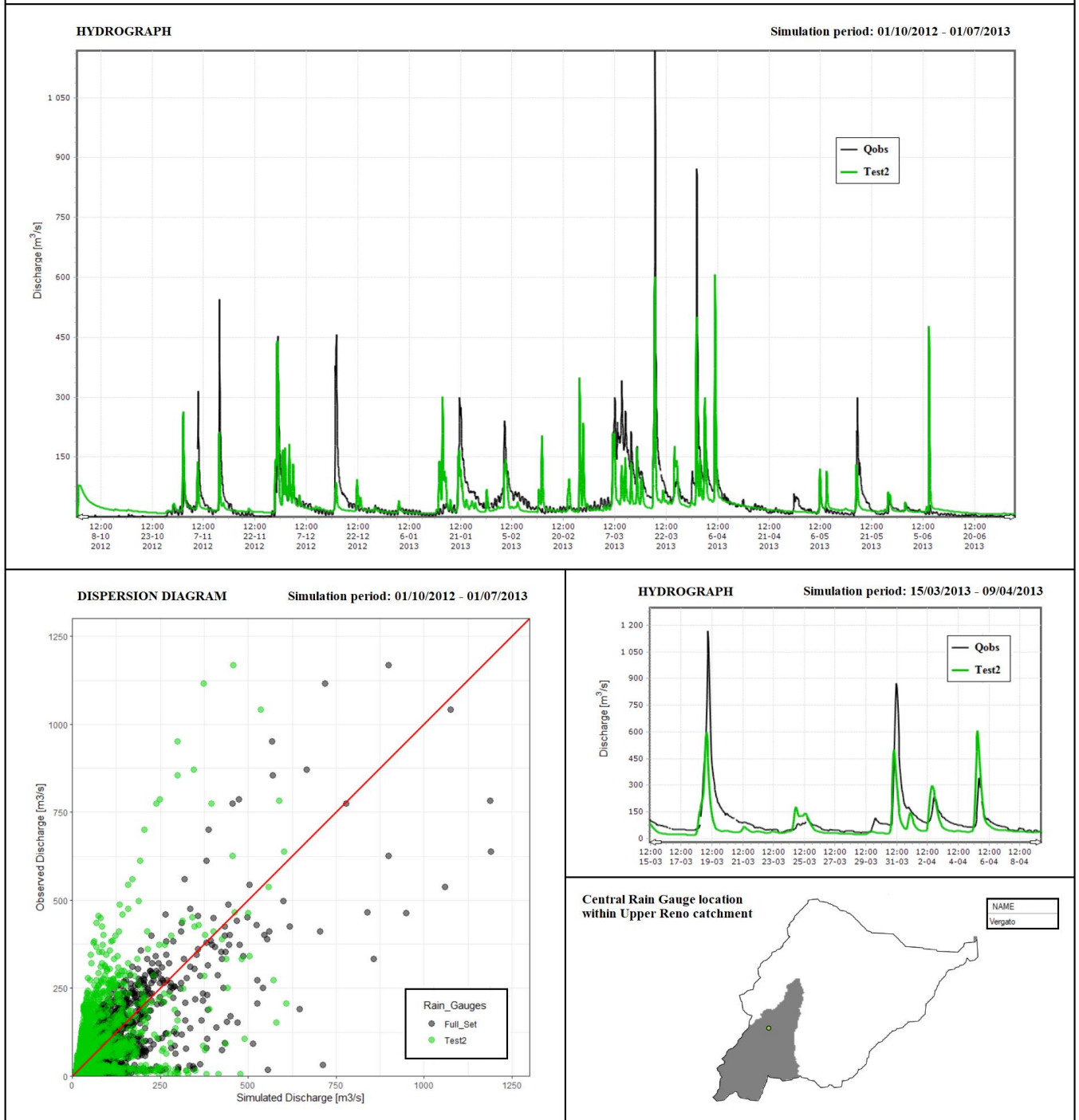
Fig.15 – Results on Test2 concerning rain gauges spatial variability within the Upper Reno catchment

7.2 EMPIRICAL APPROACHES FOR RAINFALL FORECASTING

This part of the study aims to test the model implementing a sequence of empirical prediction intervals. The methodology of this part of the study consists in the following steps:

1. identify the discharge threshold which is overtaken by 10 events in the period 2005-2013. The limit is identified at 500 m^3/s.

2. define for each event the "load" and "unload" phases: the moment in which the hydrograph starts to increase and the moment in which it returns to the previous order of magnitude (with respect to the starting time of the rain event). This time step Δt must vary from 30 to 60 hours for torrential river cases (Fig.16).

3. Out of Sample simulation: once Δt is obtained for each event, a simulation of the model is run, characterized by the substitution of the observed-rain amount within Δt with a predicted-rain quantity.

The substitution of the observed rain with a predicted one has the purpose of evaluating the predictive capability of the model without the use of forecasting data, but just on the basis of some considerations on the observed rain amount before the start of each peak event. Since this amount of "predicted-precipitation" will be constant over the whole Δt interval, we consider it as a unique variable P. Three tests are performed varying the amount of P within the interval Δt:

- Test1: P = 0
- Test2: P = average of the previous three rain values with respect to the Δt beginning
- Test3: P = the previous value with respect to Δt beginning

The results of Fig.17 show that for all ten considered events, the simulated discharge of the model under the previous hypothesis of forecasting is widely distant from both the observed discharge (Qobs) and simulated one (Qsim) (the latter obtained with the real rainfall measurements for the given period). For this reason, they cannot be taken into consideration as a possible methodology for forecasting simulation of the model.
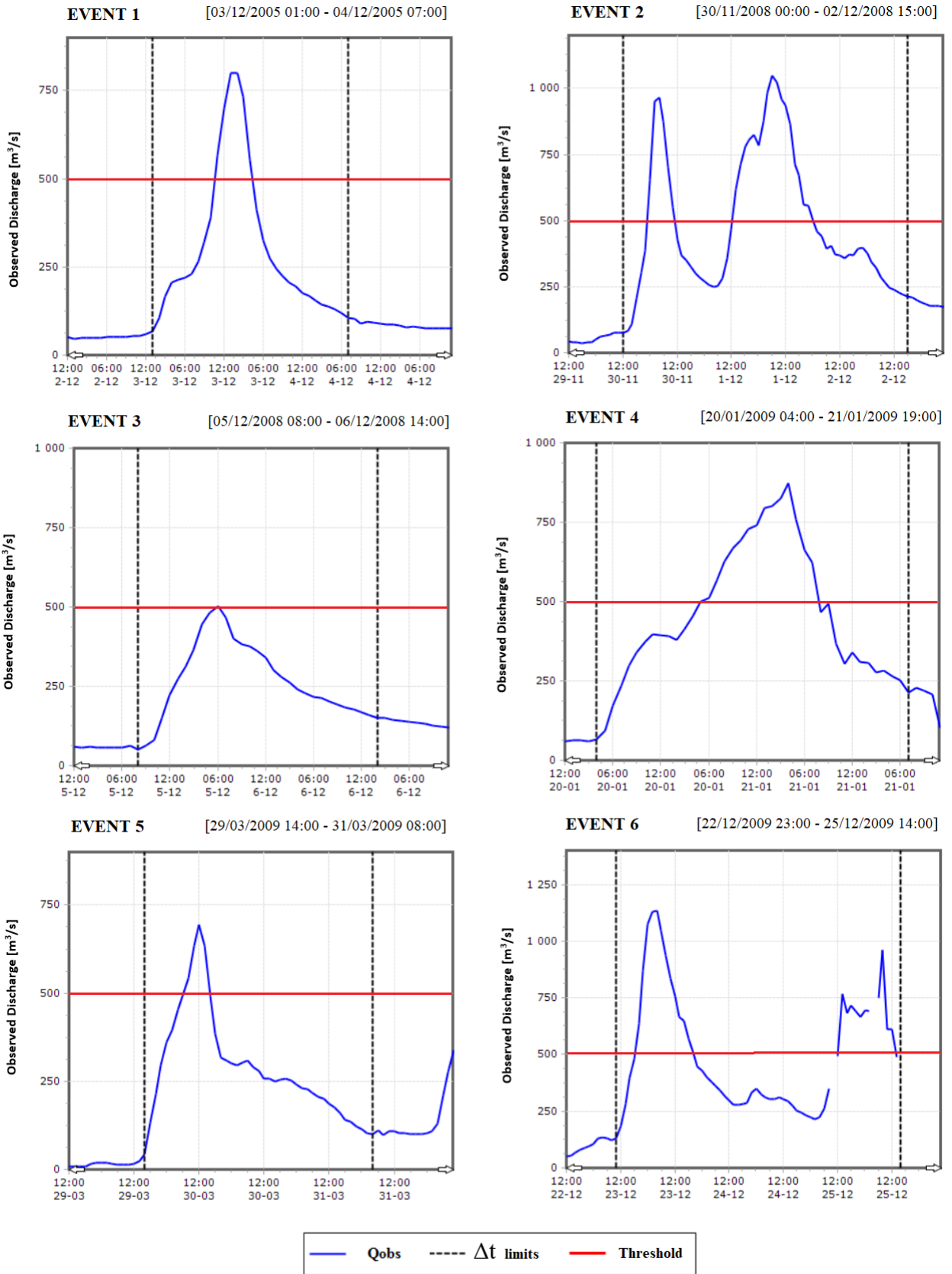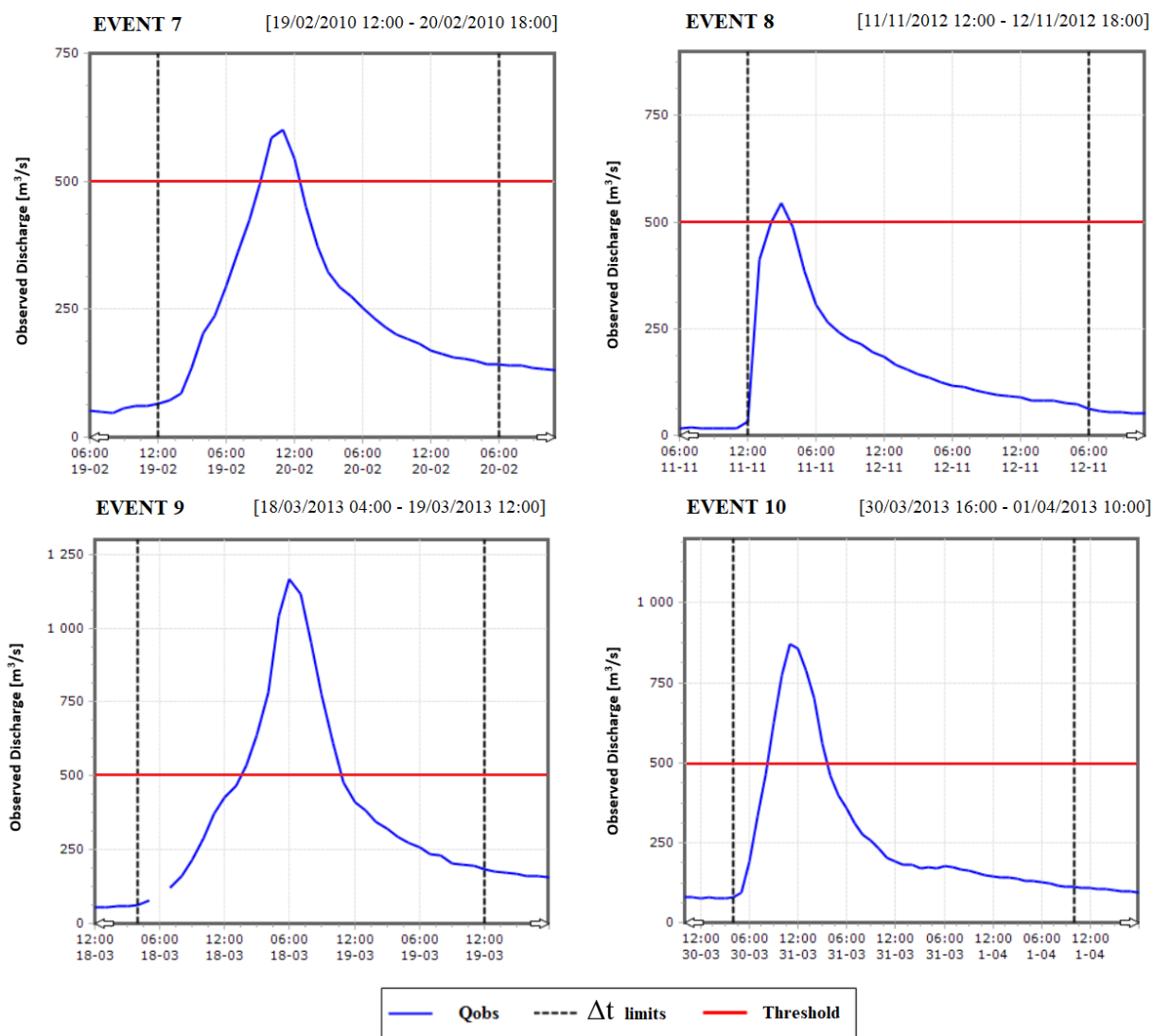
Fig.16 – identification of the 10 main events in the period 2005 – 2013. The threshold
is given by the value of 500 m³/s (horizontal red line) and the two vertical dotted lines
identifies the beginning and the end of the Δt interval.

Fig.17 - Results Out of Sample results over the ten main events between 2005 – 2013
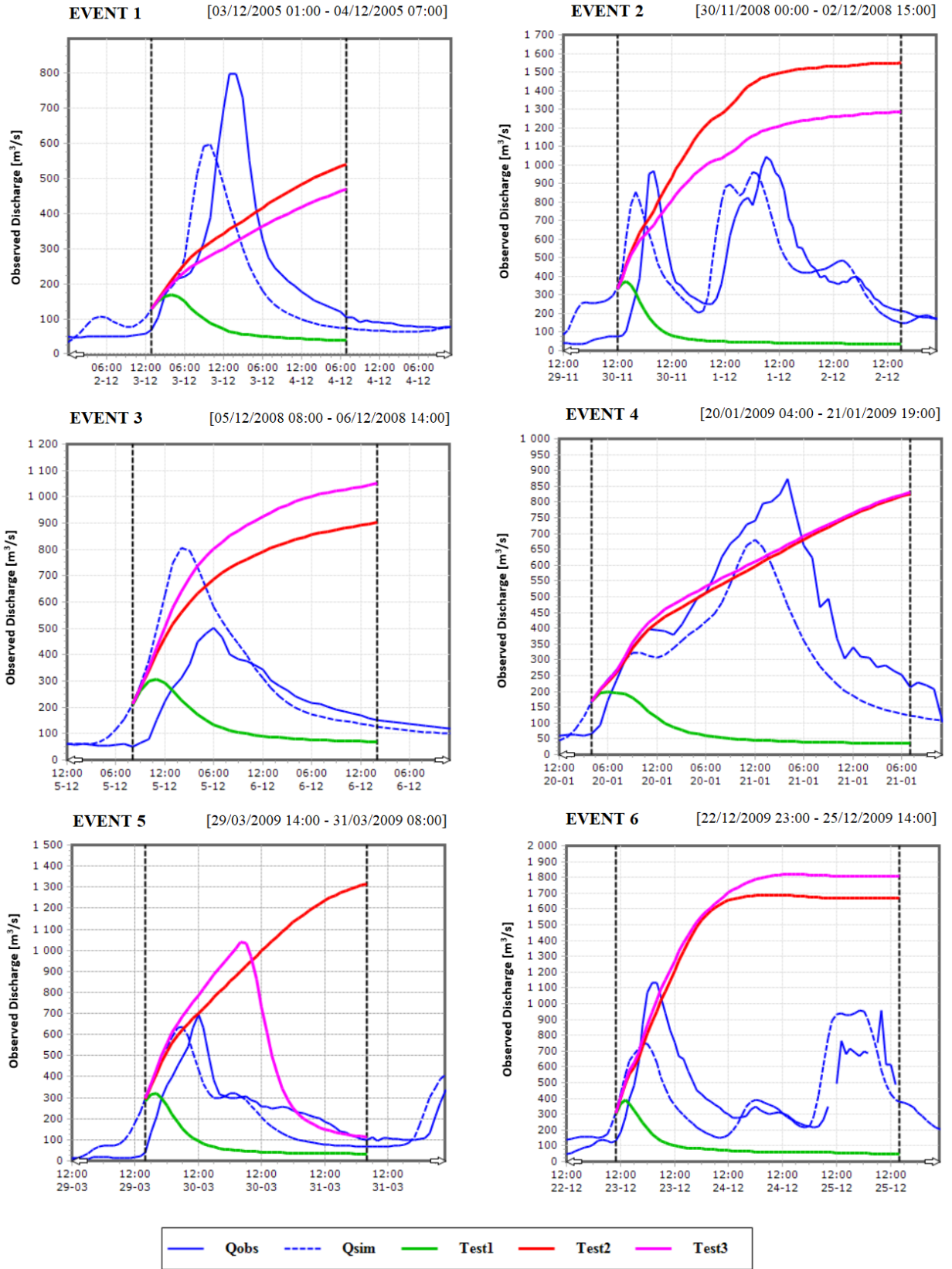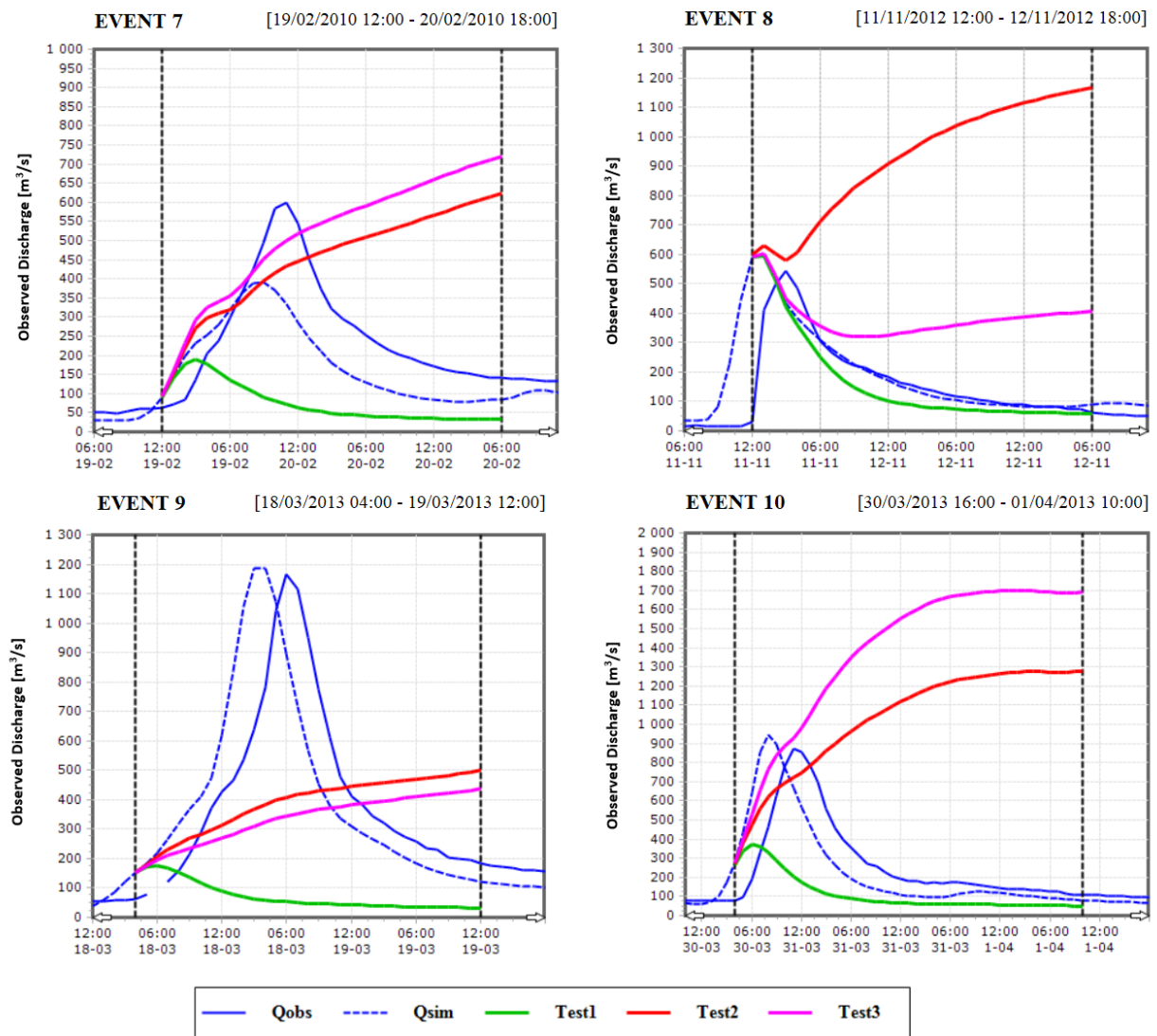
7.3 REAL TIME FORECASTING

The incorporation of quantitative precipitation forecasting (QPF) in flood warning systems with meteorological prediction has been acknowledged to play a key role, allowing an extension of the lead-time of the river flow forecast, which may enable a more timely implementation of flood control (Brath, Burlando, & Rosso, 1988). The QPF integration is particularly helpful in small and medium-sized mountainous basins like the Reno one where, given the short response time of the watershed, a precipitation forecast is necessary for an extension of the lead-time of the flood warning. It is widely recognised that obtaining a reliable QPF is not an easy task because of the complex mechanisms in the hydrological cycle governing the rainfall events (French, Krajewski, & Cuykendall, 1992), and making its forecasting difficult to quantify in time and amount. Nevertheless, this part of the study is aimed to test the response of the model to a real-time forecasting input data independently to the reliability of such precipitation.

Therefore, the current methodology consists in the use of the precipitation forecasting data obtained with the collaboration of both the regional agency ARPAE Emilia-Romagna and the company Progea Srl, referring to a data set from the 2008 to 2012 (ARPAE) and from 2012 to 2015 (Progea). Both data sets are referred to a meteorological model operating on a squared grid of 7 km per side. In order to use correctly this information, TOPKAPI subdivides this grid in a number of sub-grids such that each of the latter has a dimension equal to the cell used by the model, in this case 500m for each side.

The used data indicate the forecasted rainfall amount for a total of 24 time-step of 3-hours duration each, for a total of 72-hours lead forecasting time. Again, to standardise this information to the one used by the model so far in the study, each 3-hours single time-step is subdivided in 3 sub-steps of 1-hour duration, each with the same amount of rain.

To simulate the use of the model in real-time situation, the previous calibration configuration of the model is used. For each of the ten events identified in the previous chapter, the model uses two types of rainfall information in input: the

observed one for the period before the beginning of the main event (warm-up period), and the forecasting data for the whole Δt period. Since we are referring to events occurred some years ago with respect to the present study, for the Δt interval are both available the observed and the forecasted data. With this peculiarity it is possible to compare the forecasted discharge result with the real observed discharge and the simulated one (based on observed rainfall). With the use of a hydrograph and a dispersion diagram, the further discussions for each event identify the goodness of the forecasting results (Fig.18):

- **EVENT 1**: since no forecasting data are available in this study for the year 2005, the current event is neglected from the test.

- **EVENT 2**: The hydrograph shows that the first of two peak events is predicted in time (with an underestimation of the simulated discharge), but the second is almost completely not predicted, underlining (as depicted also from the dispersion diagram) a tendency to increasingly underestimate the simulation advancing in the lead time.

- **EVENT 3**: Even if the peak forecasted value does not correspond in time with the observed one, the amount of discharge is correctly predicted. Again, the dispersion diagram depicts a tendency to underestimate the discharge with a high lead time.

- **EVENT 4**: Almost all the event within the interval Δt is underestimated with the higher difference in correspondence of the peak observed value.

- **EVENT 5**: an initial correct development of the prediction, concerning the time in which the event occurred, is followed by an underestimation of the discharge after 20 hours of forecasting.

- **EVENT 6**: an overall underestimation trend characterized the full length of Δt, especially concerning the second peak event within the interval.

- **EVENT 7**: the strong underestimation of the peak event underlines the fact that it is not taken into account within the forecast.

- **EVENT 8**: despite the correct simulation of the first peak value, further the model simulates a rainfall over the catchment that in reality is not taking place causing an overestimation advancing in lead time.

- **EVENT 9**: the precipitation event is correctly predicted in time, but the low simulated discharge indicates that the amount of rain over the basin is strongly underestimated.

- **EVENT 10**: the diagrams illustrates as the simulation based on forecasted data correctly predicts the event both in time and peak value.

In conclusion just in one case out of ten the real-time forecasting modelling gives reliable results, depicting an overall tendency to underestimate the discharge especially as the lead time advances (generally after 20 hours of forecasting). The plots of the results display the difficulty to correctly predict rainfall events in the future, especially concerning the prediction of the amount of rain rather than the time in which it will appear.

Fig. 18 – Real-time rainfall forecasting results
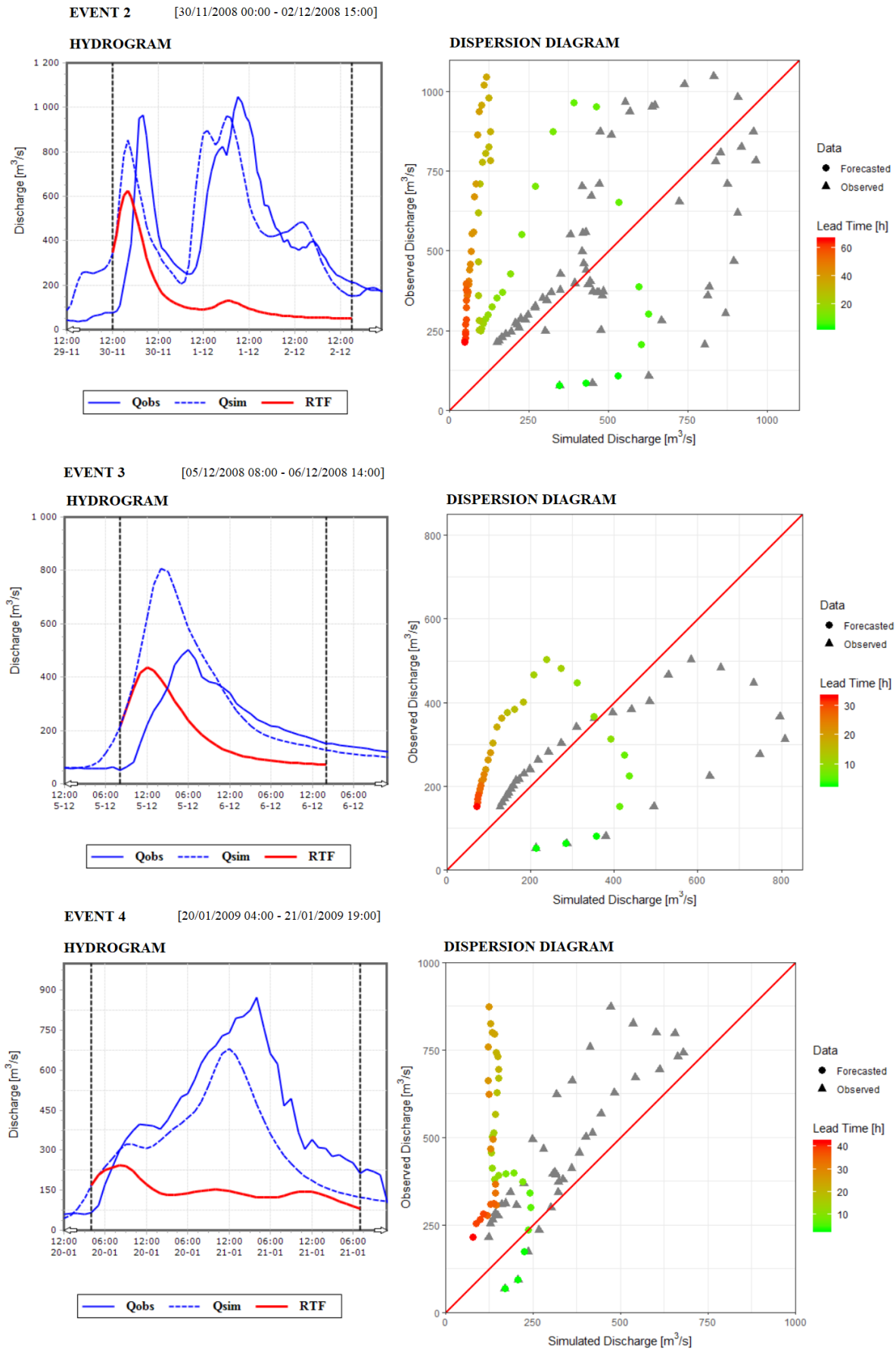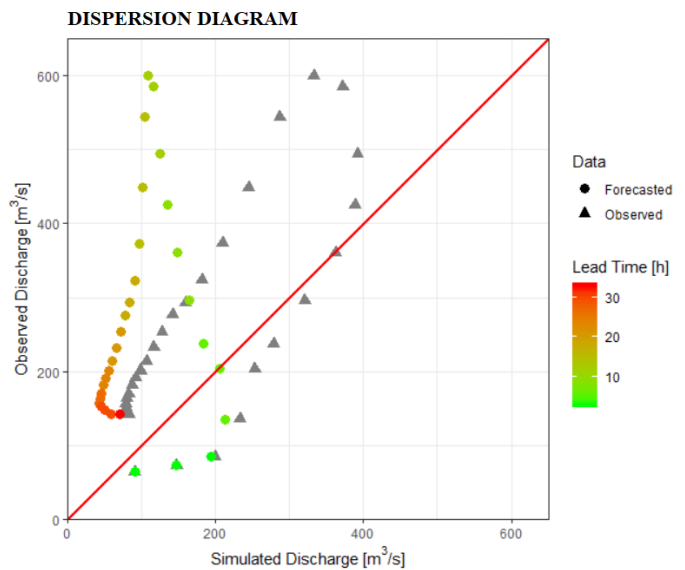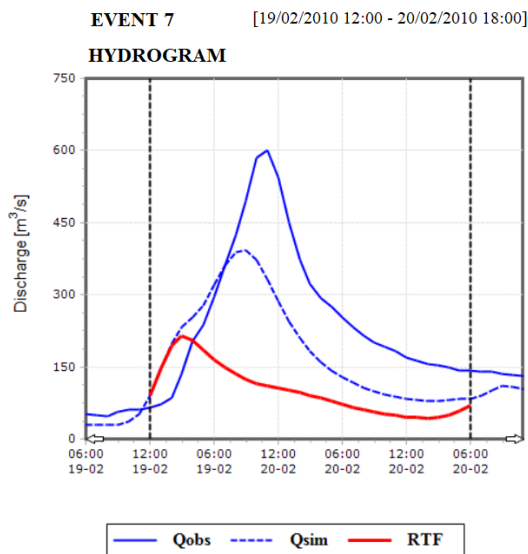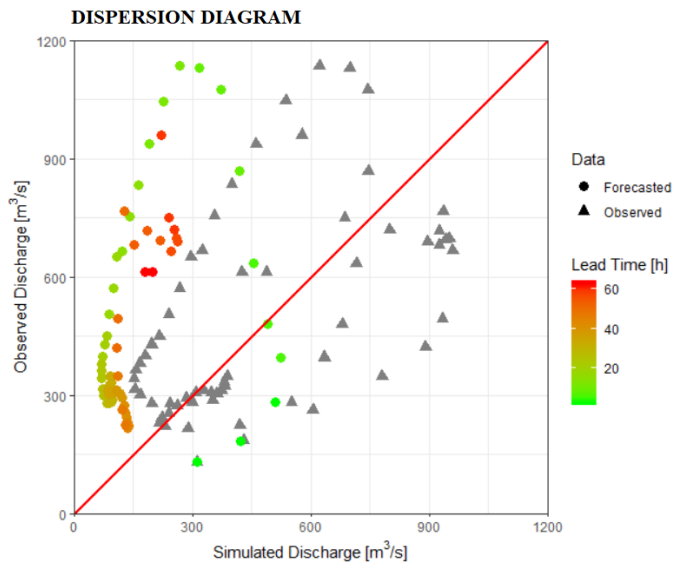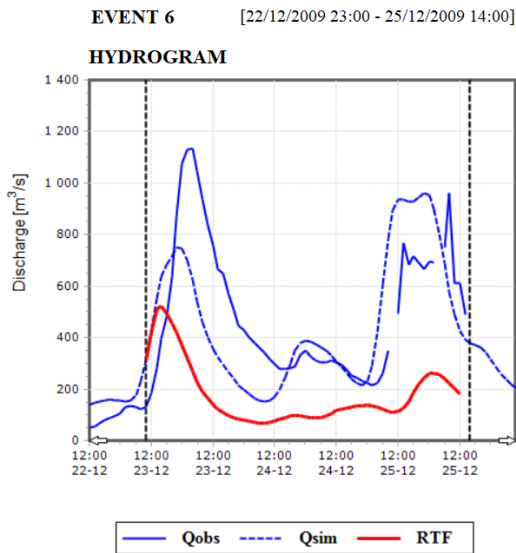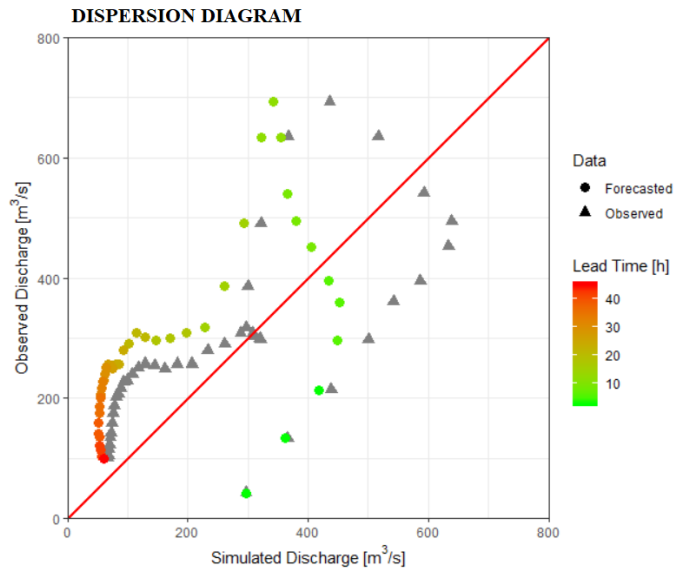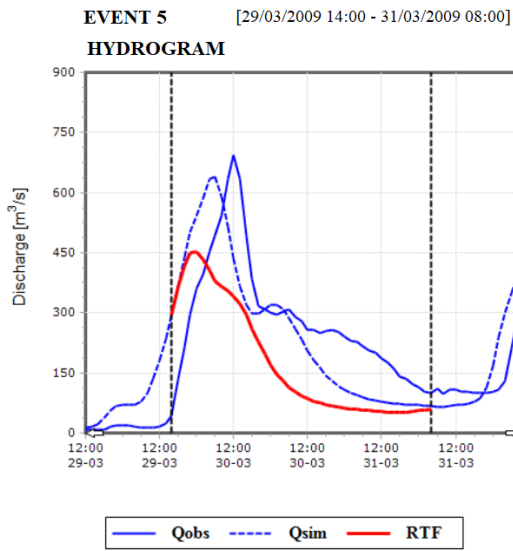
EVENT 5 [29/03/2009 14:00 - 31/03/2009 08:00]

HYDROGRAM

DISPERSION DIAGRAM

EVENT 6 [22/12/2009 23:00 - 25/12/2009 14:00]

HYDROGRAM

DISPERSION DIAGRAM

EVENT 7 [19/02/2010 12:00 - 20/02/2010 18:00]

HYDROGRAM

DISPERSION DIAGRAM

**EVENT 8**   [11/11/2012 12:00 - 12/11/2012 18:00]

HYDROGRAM
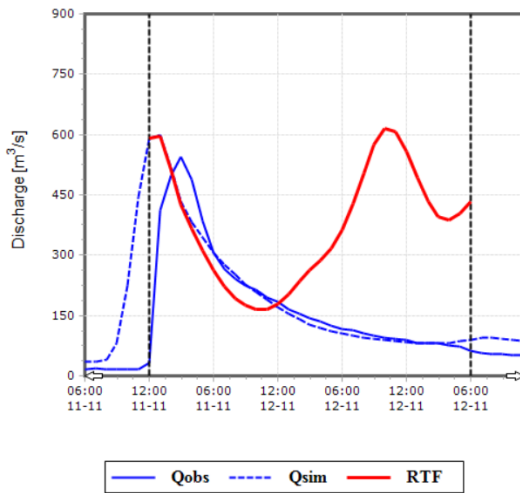
DISPERSION DIAGRAM
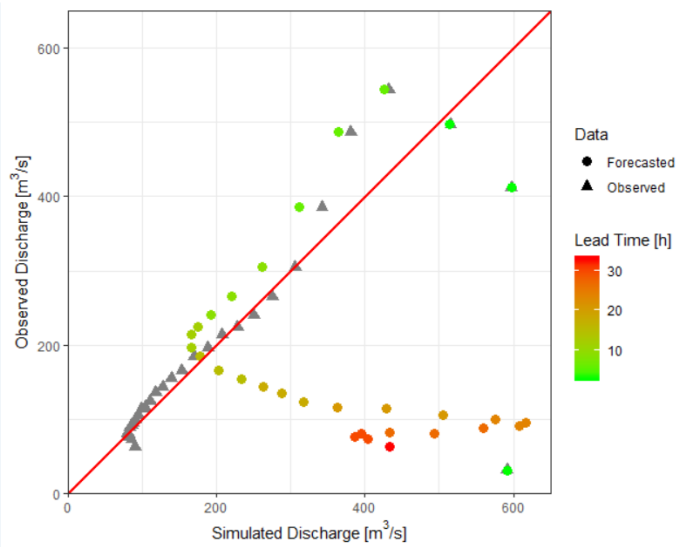
**EVENT 9**   [18/03/2013 04:00 - 19/03/2013 12:00]

HYDROGRAM
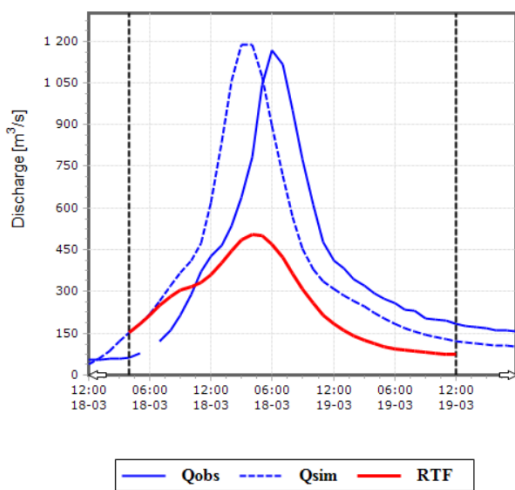
DISPERSION DIAGRAM
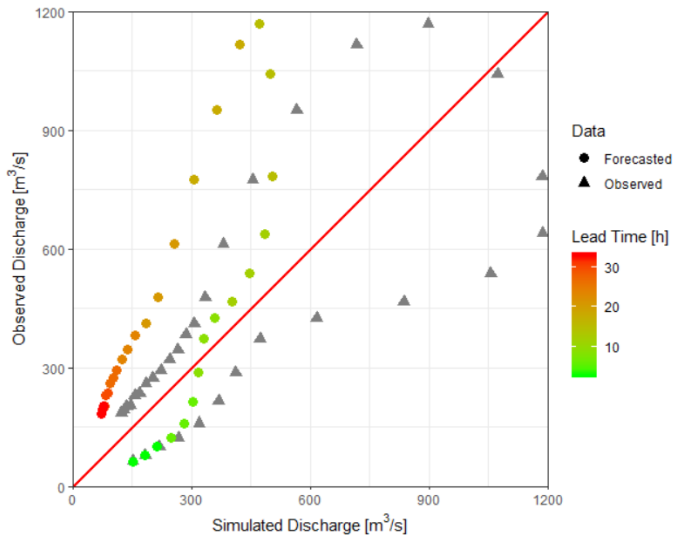
EVENT 10   [30/03/2013 16:00 - 01/04/2013 10:00]

HYDROGRAM

DISPERSION DIAGRAM

66
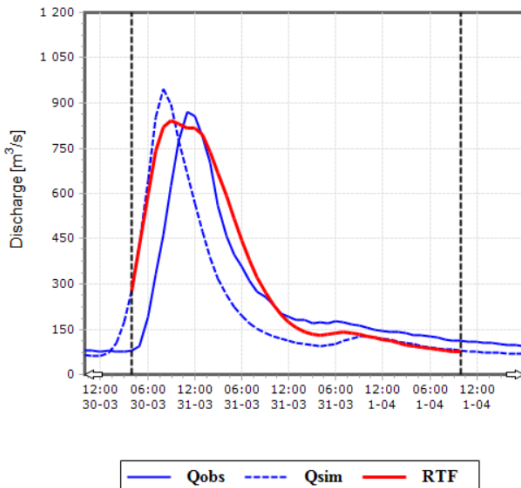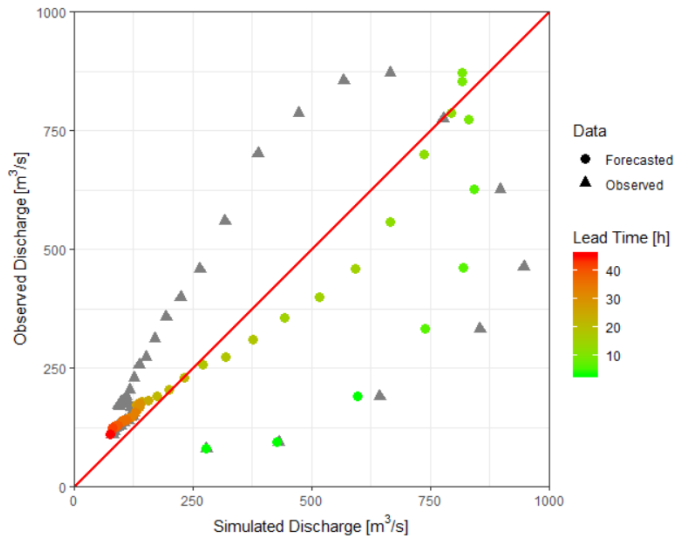
8. CONCLUSIONS

The current thesis has the purpose to test the effectiveness of the physical distributed hydrological model TOPKAPI for the sake of real-time flood forecasting for the Reno River basin. In particular rainfall forecasting, with a 72-hour time horizon, is used as input in the rainfall-runoff model for past events (selected in the period 2008-2013), with the aim of comparing the forecasted discharge with the observed one. The study demonstrates that rainfall underestimations in forecasting have a substantial impact for the flood prediction, especially if such underestimations occur in areas that are characterized by fast runoff response such as the Upper Reno catchment. Indeed, among the overall Reno catchment, just the mountainous part is considered in the study for its torrential characteristics. However, the study indicates that the considered real-time forecasting technique provides a higher flood forecasting accuracy with respect to the use of empirical prediction approaches. Moreover, the implementation of spatial variability test demonstrates that, using spatially higher resolution rainfall data, the model responds with an increase in runoff volume with respect to considering a uniform distributed rainfall event over the basin. The result, due to the interpolation of point rainfall information (inverse square distance method), demonstrates the importance of using distributed rainfall data in a fully-distributed model such as TOPKAPI if the catchment considered is characterized by torrential flood events. The combination of results in real-time forecasting and spatial variability depicts that more improvements should be pursued through more precise weather prediction models which provide timely rainfall forecasts at a temporal and spatial scale compatible with the requirements of torrential flood forecasting (Toth, Brath, & Montanari, 2000). Further research should also include the use of radar data in order to consider the spatial variability of rainfall in small and medium-sized basins (Tetzlaff & Uhlenbrook, 2005).

9. REFERENCES

Alcantara, A. (2002). *Geomorphology, natural hazards, vulnerability and prevention of natural disasters in developing countries.* Geomorphology.

Arnaud, P., Bouvier, C., Cisneros, L., & Dominguez, R. (2002). *Influence of rainfall spatial variability on flood prediction.* Journal of Hydrology.

Band, L. (1986). *Topographic partition of watershed with digital elevation models, .* Water Resour. Rees.

Bangladesh Water Development Board. (2009). *Flood Forecasting and Warning Centre.* Annual Flood Report 2010. Retrieved from http://www.ffwc.gov.bd

Barbieri, M. (n.d.). *Note storico-geografiche sul fiume Reno*. Retrieved from www.prolocogalliera.info: http://www.prolo-cogalliera.info/territorio-reno.php

Bartholomes, J., & Todini, E. (2005). *Coupling meteorological and hydrological model for flood forecasting.* Hydrol. Earth Syst. Sci.

Bell, V., & Moore, R. (2000). *The sensitivity of catchment runoff models to rainfall data at different spatial scales.* Hydrology and Earth System Sciences.

Brath, A. (1999). *On the role of numerical weather prediction models in real-time flood forecasting.* Monselice (Italy): Proceedings of the International Workshop on River Basin Modeling: Management and Flood Mitigation.

Brath, A., Burlando, P., & Rosso, R. (1988). *Sensitivity analysis of realtime flood forecasting to on-line rainfall predictions.* Perugia (Italy): Siccardi, F. and Bras, R.L.

Clapp, R., & Hornberger, G. (1978). *Empirical equations for some soil hydraulic properties.* Water Res. Res.

Cloke, H. P. (2009). *Ensemble flood forecasting; A review.* Journal of Hydrology. doi:10.1016/j.jhydrol.2009.06.005

D.Pavelli, A. (2013). *D.Pavelli, A.Capra. Climate Change and Human Impacts on Hydroclimatic Variability in the Reno River Catchment, Northern Italy.* Clean – Soil, Air, Water 2013.

Di Francesco, K. a. (2014). *Flexibility in water resources management: review of concepts and development of assessment measures for flood management systems.* Journal of the American Water Resources Association. doi:10.111/jawr.12214

Distretto Idrografico Appennino Settentrionale. (2010). *Relazione.* Art. 7 Dir. 2007/60/CE e art. 7 D.Lgs. 49/2010, ITADBI021, ITADBI901, ITADBR081.

Doorenbos, & Pruitt. (1992). *Crop water requirements.* Rome, Itlay: FAO Irrigation and Drainage.

Doorenbos, J. P. (1984). *Guidelines for predicting crop water requirements.* FAO Irrig. Drainage.

Franchini M., W. J. (1996). *Physical interpretation and sensitivity analysis of the TOPMODEL.* Journal of Hydrology.

French, M., Krajewski, W., & Cuykendall, R. (1992). *Rainfall forecasting in space and time using a neural network.* J. Hydrol.

Guzzetti, F., Stark, C., & Salvati, P. (2005). *Evaluation of Flood and Landslide Risk to the Population of Italy.* Environ. Manag.

ICHARM. (2009). *Global trends in water related disasters: an insight for policymakers.* Tsukuba, Japan: International Centre for Water Hazard and Risk Management (UNESCO). Retrieved from www.icharm.pwri.go.jp: http://icharm.pwri.go.jp

Jarvis, A., Reuter, H., Nelson, A., & Guevara, E. (2008). *Hole-filled seamless SRTM data V4.* International Centre for Tropical Agriculture (CIAT).

L. Zamboni, A. C. (2015). *La pericolosità di alluvioni nel bacino del Po e del Reno.* Ecoscienza - numero 3 .

Liu, & Todini. (2002). *Towards a comprehensive physically-based rainfall-runoff model.* Hydrology and Earth System Sciences Discussions, European Geosciences Union.

Liu, Z. (2002). *Toward a comprehensive distributed/lumped rainfall-runoff model: analysis of available physically-based models and proposal of a new TOPKAPI model. PhD dissertation.* The University of Bologna, Italy.

Liu, Z., Mario, L., & Todini, E. (2005). *Flood forecasting using a fully distributed model: application of the TOPKAPI model to the Upper Xixian catchment.* Hydrol. Earth Syst. Sci.

Martina, M., Todini, E., & Libralon, A. (2006). *A Bayesian decision approach to rainfall thresholds based flood warning.* Hydrol. Earth Syst. Sci.

O'Loughlin, G., Huber, W., & Chocat, B. (1996). *Rainfall-runoff processes and modelling.* J. Hydraul. Res.

Reno, A. d. (2002). *Piano Stralcio Assetto Idrogeologico – Rischio idraulico e assetto rete idrografica – Bacino del Fiume Reno.*

Romagna, R. E. (n.d.). *Legenda Carta dei Suoli al livello di dettaglio 1:250.000.* Retrieved from geo.regione.emilia-romagna.it: https://geo.regione.emilia-romagna.it/cartpedo/legenda.jsp?liv=3

Sigma. (2013). *Preliminary estimates for H1 2013a: Catastrophes cost global insurance industry more than USD 20 billion.* Zurich.

T.Dunne. (1978). *Rates of chemical denudation of silicate rocks in tropical cathments.* Department of Geological Science and Quaternary Research Center, University of Washington.

Tetzlaff, D., & Uhlenbrook, S. (2005). *Significance of spatial variability in precipitation for process-oriented modelling: results from two nested*

catchments using radar and ground station data. European Geosciences Union.

Todini. (1996). *The ARNO rainfall-runoff model.* J. Hydrol.

Todini, E. (1995). *New Trends in Modelling Soil Processes from Hillslope to GCM Scales. In: Oliver H.R., Oliver S.A. (eds) The Role of Water and the Hydrological Cycle in Global Change.* Springer, Berlin, Heidelberg: NATO ASI Series (Series I: Global Environmental Change).

Toth, E., Brath, A., & Montanari, A. (2000). *Comparison of short-term rainfall prediction models for real-time flood forecasting.* University of Bologna , Dipartimento di Ingegneria delle Strutture, dei Trasporti, delle Acque, del Rilevamento e del Territorio. Bologna (Italy): Journal of Hydrology.

United Kingdom Environmental Agency. (2010). *The costs of the summer 2007 floods in England.* Flood and Coastal Erosion Risk Management Research and Development Programma. Retrieved from http://publications.environmentagency.gov.uk

Weatley, G. &. (1994). *Applied Numerical Analysis .* New York, USA: Addison-Wesley.

Wikipedia, L. l. (2019, 31 jan). *Il bacino delle acque del Reno.* Retrieved from Wikipedia, L'enciclopedia libera: https://it.m.wikipedia.org/wiki/File:Bacino_idrografico_del_Reno.jpg

Woods, R. G. (2000). *Experimental design and initial results from the Mahurangi River Variability Experiment: MARVEX.* Land Surface Hydrology, Meteorology and Climate: Observations and Modeling , Water Science and Application. Lakshmi, V. ; Albertson, J.D. ; Schaake, J.

World Meteorological Organization. (n.d.). *Natural hazards - Floods and flash floods.* Retrieved from http://www.wmo.int/themes7hazards

Ringraziamenti